Theoretical Study of the Thermodynamics and Kinetics of Hydrogen Abstractions from Hydrocarbons

Aäron G. Vandeputte,[‡] Maarten K. Sabbe,[‡] Marie-Françoise Reyniers,*[,‡] Veronique Van Speybroeck,[†] Michel Waroquier,[†] and Guy B. Marin[‡]

Laboratorium voor Petrochemische Techniek, Ghent University, Krijgslaan 281 S5, B-9000 Gent, Belgium, and Center for Molecular Modeling, Ghent University, Proeftuinstraat 86, B-9000 Gent, Belgium

Received: July 2, 2007; In Final Form: August 27, 2007

Thermochemical and kinetic data were calculated at four cost-effective levels of theory for a set consisting of five hydrogen abstraction reactions between hydrocarbons for which experimental data are available. The selection of a reliable, yet cost-effective method to study this type of reactions for a broad range of applications was done on the basis of comparison with experimental data or with results obtained from computationally demanding high level of theory calculations. For this benchmark study two composite methods (CBS-QB3 and G3B3) and two density functional theory (DFT) methods, MPW1PW91/6-311G(2d,d,p) and BMK/6-311G(2d,d,p), were selected. All four methods succeeded well in describing the thermochemical properties of the five studied hydrogen abstraction reactions. High-level Weizmann-1 (W1) calculations indicated that CBS-QB3 succeeds in predicting the most accurate reaction barrier for the hydrogen abstraction of methane by methyl but tends to underestimate the reaction barriers for reactions where spin contamination is observed in the transition state. Experimental rate coefficients were most accurately predicted with CBS-QB3. Therefore, CBS-QB3 was selected to investigate the influence of both the 1D hindered internal rotor treatment about the forming bond (1D-HR) and tunneling on the rate coefficients for a set of 21 hydrogen abstraction reactions. Three zero curvature tunneling (ZCT) methods were evaluated (Wigner, Skodje & Truhlar, Eckart). As the computationally more demanding centrifugal dominant small curvature semiclassical (CD-SCS) tunneling method did not yield significantly better agreement with experiment compared to the ZCT methods, CD-SCS tunneling contributions were only assessed for the hydrogen abstractions by methyl from methane and ethane. The best agreement with experimental rate coefficients was found when Eckart tunneling and 1D-HR corrections were applied. A mean deviation of a factor 6 on the rate coefficients is found for the complete set of 21 reactions at temperatures ranging from 298 to 1000 K. Tunneling corrections play a critical role in obtaining accurate rate coefficients, especially at lower temperatures, whereas the hindered rotor treatment only improves the agreement with experiment in the high-temperature range.

1. Introduction

Many industrial processes, such as steam cracking of hydrocarbons and gas-phase polymerization of olefins, rely on radical chemistry. The reactive nature of the intermediate radicals in these processes leads to a high number of reactions. Accurate and robust modeling of radical processes requires fundamental reaction networks that can contain up to thousands of elementary reactions. Hydrogen abstraction reactions, in which a hydrogen atom is transferred from one molecule to another, often play a key part in these networks, as they have a profound effect on the product distribution. Therefore, hydrogen abstraction reactions form a substantial part of most radical reaction networks; e.g., for a steam cracking network up to 50% of the total number of reactions are H abstractions. Because most radicals are very short-lived, reliable experimental rate coefficients are hard to obtain. Furthermore, financial and instrumental limitations often restrict the feasibility to obtain experimental data for a broad range of reaction conditions and extrapolation of experimental data to the conditions of interest can lead to severe errors.

Due to increased computational capabilities and improved numerical algorithms ab initio determination of kinetic parameters has become very attractive. High-pressure limit rate coefficients can be calculated to a high level of accuracy using statistical mechanics. The most common methodology to determine these rate constants is the use of conventional transition state theory (CTST).[1] This theory is based on the assumption of quasi-equilibrium between the reactants and transition state located on the dividing surface at the saddle point of the potential energy surface. Unfortunately, the computationally simple CTST has some drawbacks, as it does not include recrossing or tunneling effects. A better approach consists of using variational transition state theory (VTST) in which the dividing surface is shifted along the reaction path to minimize the error caused by recrossing effects.[2] However, the latter methodology does not cope with tunneling effects either and can be computationally very demanding, significantly reducing its attractiveness.

Because hydrogen abstraction reactions are conceptually simple and yet play a critical role in various chemical and biochemical processes, they are among the theoretically most studied radical reactions. Detailed theoretical and experimental studies are available for the $H_2 + H^\bullet$ and the $CH_4 + H^\bullet$

[‡] Laboratorium voor Petrochemische Techniek.
[†] Center for Molecular Modeling.

10.1021/jp075132u CCC: $37.00 © 2007 American Chemical Society
Published on Web 10/30/2007

reactions.[3,4] Other well documented hydrogen abstraction reactions are the reactions involving (i) the vinyl radical $C_2H_3^{\bullet}$ and H_2,[5] (ii) the ethynyl radical $C_2H^{\bullet}$ and H_2,[6,7] (iii) the phenyl radical $C_6H_5^{\bullet}$ and H_2 or CH_4[8,9] and (iv) H abstractions between the methyl radical $CH_3^{\bullet}$ and a wide range of polyaromatics.[10] Hydrogen abstraction reactions are also frequently used as benchmarks for the development and testing of new quantum chemical methods.[11−15] Donahue et al.,[16] Zavitsas,[17−19] Blowers and Masel,[20] Ma and Schobert,[21] and Su et al.[22] have developed conceptual frameworks, often based on generalized valence bond theory, to understand reactivity patterns for this family of reactions. In particular, the empirical approach presented by Zavitsas[17] provides a quantitative description of a wide variety of H abstraction reactions over a broad range of temperatures without invoking any tunneling effects.

In this work special attention is given to the influence of tunneling on the rate coefficient. As first shown by Hund, tunneling can have an important influence on the rate coefficient of reactions in which a light particle, such as a hydrogen atom, is transferred between two heavy moieties.[23] Ever since, the literature has been flooded with methods to estimate the contribution of tunneling to the rate coefficient. In particular, transition state theory adjusted with an extra tunneling correction term has been applied successfully in the theoretical treatment of reactions involving polyatomic systems:

$$k^{\mathrm{SCTST}} = \kappa(T) k^{\mathrm{TST}} \tag{1}$$

where k^{SCTST} is the semiclassical transition state theory (SCTST) rate coefficient and κ is the transmission coefficient accounting for quantum effects such as tunneling and nonclassical reflection.

In this study we evaluate various ab initio methods by comparison of calculated thermochemical data and rate coefficients to experimental values. The objective is the selection of a reliable yet cost-effective method that can be used to study hydrogen abstraction reactions for a wide variety of applications that involve this type of reaction. In a first part of this study, four ab initio methods for the calculation of electronic energies are evaluated for a set of five hydrogen abstraction reactions. The four studied ab initio methods are the CBS-QB3 compound method of Montgomery et al.,[24] the G3B3 compound method of Baboul et al.,[25] the MPW1PW91 functional,[26] and the BMK functional.[27] In a second part of this work the influence of the 1D-HR treatment and tunneling effects on the rate coefficient is studied for a large set containing 21 hydrogen abstractions for which rate coefficients could be retrieved from the NIST Chemical Kinetics Database.[28]

2. Computational Methods

2.1. Electronic Energy Calculations. Electronic energies were calculated according to the CBS-QB3 complete basis set method,[24] the Gaussian-3 theory using B3LYP density functional theory (DFT) geometries, also denoted G3B3,[25] the Weizmann-1 (W1) method,[29,30] and two DFT methods, i.e., MPW1PW91/6-311G(2d,d,p),[26] and BMK/6-311G(2d,d,p).[27] CBS-Q, Gaussian-3, and DFT calculations were performed with the *Gaussian 03* computational package.[31] The MOLPRO 2006.1 package[32] was used to assess W1 energies.

Several studies have already indicated that for hydrogen abstractions the CBS-QB3 method offers accurate calculation of geometries and activation energies.[14,33] The CBS-QB3 complete basis set method extrapolates the MP2 energy into a full basis set energy, utilizing the asymptotic convergence of the correlation energy expanded in natural pair orbitals.[34] As the CBS-QB3 method, the G3B3 theory is a composite technique in which the total energy of a molecular species is obtained by a sequence of well-defined ab initio calculations.[25,35] G3B3 geometry optimizations and frequency calculations are performed on the B3LYP/6-31G(d) level. Electronic energies are assessed on the MP4/6-31G(d) level and corrected for basis set effects and electron correlation based on MP4 and QCISD(T) calculations. A more rigorous method to calculate electronic energies is the Weizmann-1 scheme. The W1 theory involves some computationally demanding single point calculations among which a CCSD calculation on an augmented quadruple-ζ basis set and a CCSD(T) calculation on an augmented triple-ζ basis sets. Martin and de Oliveira[29] showed that this scheme succeeds in reproducing electronic energies in the kJ mol^{-1} accuracy range for a set of 28 molecules.

In the past decade DFT methods have become a very attractive computational chemistry tool due too their low computational cost and potential high accuracy. New DFT methods are developed for various applications ranging from accurate geometry prediction to the calculation of rate coefficients. Boese and Martin[27] recently developed the BMK functional aiming for the accurate prediction of transition state properties and barrier heights. Recent studies showed that the BMK functional does not provide accurate data for radical additions and their reverse steps, β scissions.[36,37] This is probably due to the fact that the BMK test set mostly consists of hydrogen abstraction reactions.[27] Izgorodina et al.[38] reported that BMK and other DFT methods show systematic errors in the prediction of *relative* C−H bond dissociation energies, which are effectively the reaction enthalpies of hydrogen abstraction reactions. Another promising DFT method used in this work is the modified Perdew−Wang exchange functional coupled with the Perdew−Wang 91 correlation functional (MPW1PW91). Adamo and Barone[26] and de Oliveira et al.[39] showed that this functional succeeds in predicting chemical properties of first row elements close to or even better than the commonly used B3LYP method. The DFT calculations in this work were performed on a 6-311G-(2d,d,p) basis set.

2.2. Rate Coefficient Calculations. Rate coefficients are calculated using the conventional transition state theory in the high-pressure limit:

$$k_{\infty}(T) = \kappa(T) \frac{k_{\mathrm{B}}T}{h} \frac{n_{\mathrm{opt},\ddagger} q_{\ddagger}}{n_{\mathrm{opt,A}} q_{\mathrm{A}} n_{\mathrm{opt,B}} q_{\mathrm{B}}} \mathrm{e}^{-\Delta^{\ddagger}E/RT} \tag{2}$$

with q the total molar partition function per unit volume, $\Delta^{\ddagger}E$ the zero point corrected electronic activation barrier, and $\kappa(T)$ the transmission coefficient accounting for quantum mechanical effects. The partition functions are calculated for a single optical isomer, and all existing configurations, including those that are not thermally accessible from the reference configuration, should be accounted for. As each optical isomer represents a distinct but energetically equivalent state, a correction n_{opt} enters into eq 2. External and internal symmetry numbers are contained within the partition functions.

In this study, ab initio rate coefficients are compared with experimental results. As a measure for the deviation between both values we opted to define a factor ρ according to

$$\rho = \begin{cases} \dfrac{k_{\mathrm{calc}}}{k_{\mathrm{exp}}} & k_{\mathrm{calc}} > k_{\mathrm{xp}} \\ \dfrac{k_{\mathrm{exp}}}{k_{\mathrm{calc}}} & k_{\mathrm{exp}} > k_{\mathrm{calc}} \end{cases} \tag{3}$$

The factor ρ is a value larger than 1 and gives a proper indication for the relative deviation between both rate coefficients. Average $\langle\rho\rangle$ values for a set of reactions are weighted over the number of experiments to prevent giving more weight to reactions with multiple experimental data:

$$\langle\rho\rangle = \sum_{i}^{n_{\text{reac}}} \frac{1}{n_{\text{reac}}} \sum_{j}^{n_{\text{exp},i}} \frac{1}{n_{\text{exp},i}} \rho_{i,j} \tag{4}$$

with n_{reac} the number of reactions, $n_{\text{exp},i}$ the number of experiments for reaction i, and $\rho_{i,j}$ equal to the factor ρ of experiment j for reaction i. The IUPAC task group on "Selected free radicals and critical intermediates: thermodynamic properties from theory and experiment" suggests that the uncertainty factor on calculated rate coefficients for a set of reactions should be defined as twice $\langle\rho\rangle$.[40]

Kinetic parameters were obtained from linear least-square regression on the Arrhenius model:

$$\ln k = \ln A - \frac{E_a}{RT} \tag{5}$$

with k sampled at intervals of 50 K between $T - 100$ and $T + 100$ K, with T the temperature of interest.

2.3. Partition Functions. Partition functions are calculated on the B3LYP/6-311G(2d,d,p) level within the CBS-QB3 method, the B3LYP/6-31G(d) level within the G3B3 method, and the MPW1PW91/6-311G(2d,d,p) or BMK/6-311G(2d,d,p) level for respectively the MPW1PW91 and BMK DFT methods. The default scaling factor of 0.96 and 0.99 was used for respectively the G3B3 and CBS-QB3 method. For the MPW1PW91 and BMK method a scaling factor of 0.99 was applied, which is close to the value of 0.9877 advised by Andersson and Uvdal for scaling of DFT/triple-ζ ZPVEs.[41]

Although the harmonic oscillator (HO) approximation is very convenient, it breaks down for large-amplitude internal motions, such as internal rotations. The influence on the rate coefficient of internal rotations that exist in both the reactants and the transition state is limited as their contributions cancel out in eq 2. Internal rotations that do not cancel out in eq 2 can have an important influence and should be treated as accurately as possible. This pertains in particular to the rotation about the axis containing the breaking and forming C−H bond in the transition state. This internal mode is treated as a 1D hindered internal rotor (1D-HR) by solving the Schrödinger equation for the internal rotation using the methodology and code developed by Van Speybroeck et al.[42] which was later on validated.[43−45] In this procedure, the B3LYP/6-31g(d) energy profile for internal rotation is regressed to a third-order Fourier series and the exact reduced moment of inertia for one single rigid internal rotation (I(3,4) according to the nomenclature introduced by East and Radom[46]) is applied. It has been shown that the 1D-HR treatment of this particular internal rotor in the transition state has a much larger influence on the rate coefficient than the hindered rotor treatment of the other internal rotors present in the transition state and reactants.[47]

2.4. Transmission Coefficients. ***2.4.1. Zero Curvature Tunneling.*** Tunneling of the migrating hydrogen atom through the reaction barrier can be evaluated by several one-dimensional methods, i.e., the methods of Wigner,[48] Skodje et al.,[49] and Eckart.[50] These zero curvature tunneling methods (ZCT) are based on the assumption that the reaction and tunneling path coincide leading to simple algebraic expressions for the transmission coefficient and thus making these tunneling methods computationally very attractive.

The Wigner method is the most basic approximation to account for tunneling of a particle through the reaction barrier.[48] Assuming a parabolic potential for nuclear motion near the transition state, the transmission coefficient $\kappa(T)$ can be obtained from perturbation theory:

$$\kappa(T) = 1 + \frac{1}{24}\left(\frac{h\,\text{Im}(\nu^{\ddagger})}{k_B T}\right)^2 \tag{6}$$

Equation 6 is valid for $k_B T \gg h\,\text{Im}(\nu^{\ddagger})$. For hydrogen abstraction reactions with a typical imaginary wavenumber of 1500 cm^{-1}, $k_B T$ equals $h\,\text{Im}(\nu^{\ddagger})$ at a temperature as high as 2160 K. This is a first indication that the Wigner method will lack accuracy in predicting tunneling contributions at temperatures of practical interest (e.g., 298, 600, and 1000 K).

In contrast to the Wigner method, the method of Skodje and Truhlar depends not only on the imaginary frequency but also on the height of the potential energy barrier.[49] The authors assumed a parabolic approximation to the minimum energy path (MEP). Calculation of the exponential damping of waves tunneling through this energy barrier leads to thermally averaged transmission coefficients that are given with good accuracy by the following analytic expressions:

$$\beta \le \alpha: \qquad \kappa(T) = \frac{\beta\pi/\alpha}{\sin(\beta\pi/\alpha)} - \frac{\beta}{\alpha - \beta} e^{[(\beta-\alpha)(\Delta V^{\ddagger} - V)]}$$

$$\beta \le \alpha: \qquad \kappa(T) = \frac{\beta}{\beta - \alpha}(e^{[(\beta-\alpha)(\Delta V^{\ddagger} - V)]} - 1) \tag{7}$$

with $\alpha = 2\pi/[h\,\text{Im}(\nu^{\ddagger})]$ and $\beta = (k_B T)^{-1}$.

The Eckart method[50] is similar to the one proposed by Skodje and Truhlar[49] and also accounts for the barrier height, but here an Eckart potential is fitted to the energies of three stationary points, i.e., the zero-point-corrected energies of the reactants ($s = -\infty$), the saddle point ($s = s_0$), and the products ($s = +\infty$):

$$V(s) = \frac{\alpha e^{\alpha(s-s_o)}}{1 + e^{\alpha(s-s_o)}} + \frac{b e^{\alpha(s-s_o)}}{(1 + e^{\alpha(s-s_o)})^2} + c \tag{8}$$

where s is the reaction coordinate and a, b, c, α, and s_o are parameters that can be calculated from the classical potential energies at the reactants, saddle point, and products and from the imaginary frequency (see Appendix A). As for the method of Skodje and Truhlar,[49] the Schrödinger equation accounting for tunneling can be solved exactly for this type of reaction barrier, allowing the construction of an analytical expression for of the transmission probability. To determine the tunneling coefficient, the expressions presented by Schwartz et al. were adopted.[51] This yields for the width parameter Δ of the Eckart function:

$$\Delta = \frac{i}{2\pi c\,\text{Im}(\nu^{\ddagger})}\left[\frac{1}{8}\frac{(B^2 - A^2)^2}{A^3}\right]^{1/2} \tag{9}$$

with $A = [(V_F)^{0.5} + (V_R)^{0.5}]^2$, $B = V_F - V_R$ with V_F the forward and V_R the reverse barrier. The transmission probability P as a function of the energy E of the colliding reactants can then be written as

$$P(E) = 1 - \frac{\cosh(\alpha - \beta) + \cosh(\delta)}{\cosh(\alpha + \beta) + \cosh(\delta)} \tag{10}$$

with $\alpha = (4\Delta\pi^2/h)(2E)^{0.5}$, $\beta = (4\Delta\pi^2/h)(2E - B))^{0.5}$, and $\delta = (4\Delta\pi^2/h)[2A - (h^2/16\pi^2\Delta^2)]^{0.5}$.

In this work the tunneling coefficient is retrieved by integrating the Boltzmann weighted transmission probability (eq 11) using an 11-point Newton−Cotes quadrature formula.

$$\kappa(T) = \frac{e^{V_F/k_BT}}{k_BT}\int_0^\infty P(E)e^{-E/k_BT}\,dE \tag{11}$$

The standard calculation in Gaussian of the imaginary frequency ($\mathrm{Im}(\nu^{\ddagger})$) involves the reduced mass μ_{red}:

$$\mathrm{Im}(\nu^{\ddagger}) = \frac{1}{2\pi}\left(\frac{|F^{\ddagger}|}{\mu_{red}}\right)^{0.5} \tag{12}$$

whereas rather the effective reduced mass μ_{eff} should be used, accounting for corner cutting of the tunneling path at larger curvatures of the minimum energy path. This corner cutting is caused by the negative internal centrifugal character of tunneling systems. In regions where the reaction path shows large curvature, tunneling systems tend to cut the corner to minimize the exponential damping of the wave-particle package as it traverses the classical forbidden area. To account for these effects, the effective reduced mass μ_{eff} was calculated according to the approximation given by Gonzalez et al. for infinitesimal displacements in the vicinity of the transition state:[52]

$$\mu_{eff} = [\vec{v}_{\ddagger}^{T}\cdot M\cdot \vec{v}_{\ddagger}] \tag{13}$$

with $\vec{v}_{\ddagger}^{T}$ the eigenvector corresponding to the negative eigenvalue of the Hessian matrix at the transition state and M a $3N \times 3N$ diagonal matrix with the atomic masses along the diagonal.

2.4.2. Small Curvature Tunneling Methods. As zero curvature tunneling (ZCT) methods do not account for the corner cutting effect, they tend to underestimate tunneling probabilities. More advanced tunneling methods are based on the inclusion of deviations between the tunneling path and the reaction path. These tunneling methods are often computationally demanding as they require information about the potential energy, the potential energy gradient and Hessian along the reaction path. In this work the centrifugal dominant small curvature semiclassical (CD-SCS) tunneling method is applied on two reactions and compared with the ZCT methods.

To obtain the CD-SCS tunneling corrections the imaginary action integral (eq 14) has to be evaluated along a tunneling path that follows a curve between the concave-side classical turning points in the direction of the reaction path curvature vector:

$$\theta(E) = \frac{2\pi}{h}\int_{s_1}^{s_2}\sqrt{2\mu_{red}|E - V(s)|}\,ds \tag{14}$$

Consider ξ the distance along the small-curvature tunneling path, $t(s)$ the distance between the considered tunneling path and the MEP at s, and $\kappa(s)$ the curvature at s, then it can be shown using analytical geometry that

$$d\xi = \sqrt{[1 - a(s)]^2 + \left[\frac{dt(s)}{ds}\right]^2}\,ds \tag{15}$$

with

$$a(s) = |\kappa(s)\,t(s)| \tag{16}$$

and $\kappa(s)$ the magnitude of the curvature:

$$\kappa(s) = \left(\sum_{i=1}^{F-1}[\kappa_i(s)]^2\right)^{1/2} \tag{17}$$

In eq 17 the summation is over all modes ($F = 3N - 6$) with exclusion of the mode that corresponds with the motion along the reaction path. κ_i is the reaction path curvature of mode i and is given by

$$\kappa_i(s) = \vec{L}_i^{T}F\frac{\nabla\vec{V}}{|\nabla\vec{V}|^2} \tag{18}$$

In eq 18 $\vec{L}_i^{T}$, F, and $\nabla\vec{V}$ are respectively the transpose of the generalized normal mode eigenvector of mode i, the force constant matrix or Hessian matrix, and the gradient of the potential energy. Within the harmonic oscillator approximation Truong found that $t(s)$ is given by[53]

$$t(s) = \left(\frac{\kappa\hbar}{\mu_{red}}\right)^{1/2}\left(\sum_{m}^{F-1}[\kappa_m(s)]^2\omega_m{}^2(s)\right)^{-1/4} \tag{19}$$

The imaginary action integral along the small-curvature tunneling path is defined as

$$\theta(E) = \frac{2\pi}{h}\int_{\xi_1}^{\xi_2}\sqrt{2\mu_e|E - V(\xi(s))|}\,d\xi \tag{20}$$

Combining eqs 14, 15, and 20 yields the effective reduced mass:

$$\mu_{eff} = \mu_{red}\left[[1 - a(s)]^2 + \left[\frac{dt(s)}{ds}\right]^2\right] \tag{21}$$

To make the method generally applicable, even when $t(s)$ is greater than or equal to the radius of curvature of the reaction path, μ_{eff} is approximated by[54]

$$\mu_{eff} = \mu_{red} \times \min\begin{cases}\exp\left\{-2a(s) - a(s)^2 + \left(\frac{dt(s)}{ds}\right)^2\right\}\\ 1\end{cases} \tag{22}$$

Substitution of eq 22 in eq 14 and evalution of this imaginary action integral along the MEP yields transmission probabilities from which the tunneling coefficient can be calculated.

To obtain CD-SCS tunneling coefficients an intrinsic reaction coordinate (IRC) calculation was performed using the B3LYP/6-311G(2d,d,p) method. The reaction path was calculated along 150 points in both directions of the reaction coordinate with a step size of 0.01 bohr amu$^{1/2}$. From the IRC calculation the gradient $\nabla\vec{V}(s)$ along the reaction path was retrieved. For every point along the reaction path a frequency analysis was performed using the same level of theory B3LYP/6-311G(2d,d,p). This yielded information about the Hessian, normal-mode frequencies and displacements. With this information the effective reduced mass along the reaction path could be obtained. Next, the imaginary action integral (eq 14) was evaluated using the midpoint rule for discrete integration, yielding $\theta(E)$ from which the transmission probabilities are calculated as

$$P_{quantum}(E) = \frac{1}{1 + e^{2\theta(E)}} \tag{23}$$

Finally, the transmission coefficient is obtained by deviding the Boltzmann weighted quantummechanical transmission probability by the Boltzmann weighted classical transmission probability:

$$\kappa(T) = \frac{\int_{E=0}^{\infty} P_{\text{quantum}}(E) e^{-E/k_B T}\, dE}{\int_{E=0}^{\infty} P_{\text{classic}}(E) e^{-E/k_B T}\, dE} = \frac{e^{E^{\ddagger}/k_B T}}{k_B T} \int_{E=0}^{\infty} P_{\text{quantum}}(E) e^{-E/k_B T}\, dE \quad (24)$$

3. Results and Discussion

3.1. Influence of the Level of Theory. In this section the accuracy of four ab initio methods in predicting thermochemical reaction properties of hydrogen abstraction reactions is studied. Five hydrogen abstractions were selected for which sufficient experimental data could be retrieved concerning the standard reaction enthalpy $\Delta_r H°(298\ \text{K})$, standard reaction entropy $\Delta_r S°(298\ \text{K})$ and rate coefficient. The five considered reactions are

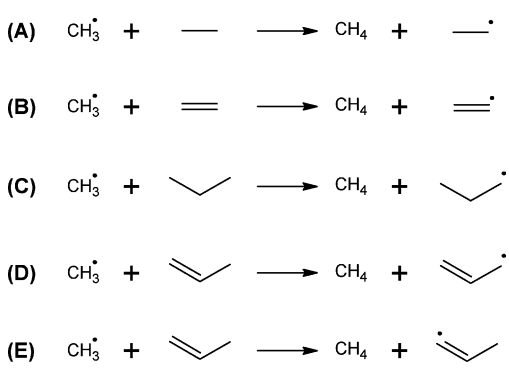

HO thermochemical properties for these five reactions were calculated within the CBS-QB3, G3B3, MPW1PW91/6-311G(2d,d,p), and BMK/6-311G(2d,d,p) methods, and the results are presented in Table 1. The calculated standard reaction enthalpies and standard reaction entropies are expressed relative to experimental data, and the CBS-QB3 barriers were taken as reference for the calculated reaction barriers $\Delta^{\ddagger}E(0\ \text{K})$. The energy barriers reported in this study include ZPVE.

From Table 1 it is seen that the four studied levels of theory provide accurate standard reaction enthalpies for the five reactions of the set. The results in Table 1 follow the general expectations. A more negative $\Delta_r H°(298\ \text{K})$ points toward a more exothermic reaction and hence a more stable radical formed after H abstraction. Table 1 illustrates that an allylic radical is more stable than a secondary carbon radical, which in his turn is more stable than a vinylic radical.[55] The best agreement with experimental standard reaction enthalpies is obtained with the two composite methods, i.e., CBS-QB3 and G3B3, which yield a MAD of respectively 3.1 and 2.1 kJ mol^{-1}. The BMK functional (MAD = 3.6 kJ mol^{-1}) performs slightly better than the MWP1PW91 functional (MAD = 4.2 kJ mol^{-1}) and yields results that have accuracy similar to those obtained with the CBS-QB3 method. The same conclusions were also drawn by Izgorodina et al.[38] who found that the BMK functional predicts equally accurate relative bond dissociation energies for C−H bonds compared to high-level composite methods. For standard reaction entropies, the best agreement with experimental values is obtained with the BMK functional (MAD = 3.3 J mol^{-1} K^{-1}). This is somewhat surprising as Boese and Martin[27] showed that the performance of the BMK functional in predicting vibrational frequencies of non transition state structures was slightly worse than that of the B3LYP method. The other three methods yield similar accuracies in the prediction of standard reaction entropies with a MAD ranging between 3.9 and 4.0 J mol^{-1} K^{-1}. It is seen that all four methods overestimate $\Delta_r S°(298\ \text{K})$ for reaction **A** with at least 10 J mol^{-1} K^{-1}. This deviation was found to be mainly due to an overestimation of the standard entropy of the ethyl radical with 8 kJ mol^{-1}, caused by the failing HO approximation in describing the free rotation about the C−C bond for this radical. A positive standard reaction entropy indicates that the reactants have a higher potential to store energy in internal modes. The highly negative $\Delta_r S°(298\ \text{K})$ for reaction **D** results both from symmetry effects (i.e., the products of this reaction have a higher symmetry number than the corresponding reactants) and from the high barrier to internal rotation in the allyl radical caused by resonance effects. In the last section of Table 1 the BMK, MPW1PW91, and G3B3 reaction barriers are compared to the CBS-QB3 barriers. Best agreement with the CBS-QB3 barriers is obtained with the BMK functional, reflecting the fact that this functional aims for the accurate prediction of transition state barriers and is founded on a test set that mostly consists out of hydrogen abstraction reactions. The MAD between both methods amounts to only 1.0 kJ mol^{-1}. It is also seen that the G3B3 barriers are on average 6.6 kJ mol^{-1} higher than the CBS-QB3 values; the MPW1PW91 method on the other hand predicts barriers that are almost 10 kJ mol^{-1} lower.[14]

To study the influence of tunneling effects and internal rotation about the forming/breaking transition state bond, rate coefficients were calculated for the set of five reactions according to the HO approximation, the 1D-HR scheme without tunneling corrections, and the 1D-HR scheme corrected for tunneling according to Wigner (1D-HR/W), Skodje and Thrular (1D-HR/S&T), and Eckart (1D-HR/E) at 298, 600, and 1000 K. The rate coefficients, calculated with the four different levels of theory under study, were compared to experimental results. As mentioned before, the factor ρ is considered as a measure for the deviation between experimental and calculated values. The results are shown in Table 2 together with the arithmetic mean value of $\langle\rho\rangle$ over the three temperatures under study. It is seen that with the MPW1PW91 functional the best agreement with experiment is obtained within the 1D-HR approximation without tunneling contribution. For this functional it is found that tunneling contributions do not improve the agreement with experiment, even at temperatures as low as 298 K. This indicates that the MPW1PW91 rate coefficients are too high, probably due to an underestimation of the reaction barrier. Best performance within the G3B3 method is obtained for the 1D-HR/S&T treatment. For this method large ρ values are obtained especially at lower temperatures. Calculated HO rate coefficients with the G3B3 method at 298 K are often more than 3 orders too small. This originates from an overestimation of the reaction barriers within this methodology. The BMK and CBS-QB3 method perform well with a $\langle\rho\rangle$ value of respectively 9.3 and 8.5. For both methods best agreement with experiment is obtained within the 1D-HR/E scheme.

From the results in Table 2, it was concluded that the CBS-QB3 method provides the best agreement with experiment, closely followed by the BMK method. As mentioned above, the G3B3 and MPW1PW91 theory failed to yield accurate rate coefficients due to less accurate barrier heights. The good result obtained with the CBS-QB3 method could also be attributed to compensating effects such as, for example, an overestimating of the tunneling contribution compensated by a systematically too high reaction barrier. Therefore the accuracy in barrier prediction of the CBS-QB3 method was further investigated. Two small reaction systems were selected on which high-level Weizmann-1 calculations could be performed[29,30] and compared with reaction barriers predicted by the four other levels of theory

TABLE 1: Comparison of Thermochemical Data for a Set Containing Five H Abstractions Calculated with the CBS-QB3, G3B3, MPW1PW91/6-311G(2d,d,p), and BMK/6-311G(2d,d,p) Methods within the HO Approximation

	reaction					
	A	**B**	**C**	**D**	**E**	MAD
$\Delta_r H°_{exp}$(298 K) [kJ mol^{-1}]						
NIST + CRC	−17.8	26.0	−15.9	−70.0	26.0	
$\Delta_r H°$(298 K) − $\Delta_r H°_{exp}$(298 K) [kJ mol^{-1}]						
CBS-QB3[b]	+2.3	−4.2	+1.5	−6.1	−1.3	3.1
G3B3[c]	+4.0	−1.7	+3.3	−0.5	+1.2	2.1
MPW1PW91[d]	−1.1	−6.1	−1.9	−8.9	−2.8	4.2
BMK[e]	+0.0	−6.3	−0.5	−7.7	−3.4	3.6
$\Delta_r S°_{exp}$(298 K) [J mol^{-1} K^{-1}]						
NIST + Benson	8.6	9.6	7.2	−15.0	−2.2	
$\Delta_r S°$(298 K) − $\Delta_r S°_{exp}$(298 K) [J mol^{-1} K^{-1}]						
CBS-QB3[b]	+11.8	−3.6	+2.5	−0.7	−1.3	4.0
G3B3[c]	+10.4	−4.3	+1.9	−1.0	−2.0	3.9
MPW1PW91[d]	+11.3	−3.8	+2.4	−0.8	−1.6	4.0
BMK[e]	+9.9	−3.4	+2.3	+0.5	−0.6	3.3
$\Delta^{\ddagger}E$ (0 K) [kJ mol^{-1}]						
CBS-QB3[b]	58.9	69.4	58.0	43.0	69.4	
$\Delta^{\ddagger}E$(0 K) − $\Delta^{\ddagger}E_{CBS-QB3}$(0 K) [kJ mol^{-1}]						
G3B3[c]	+6.9	+6.3	+6.7	+6.6	+6.6	6.6
MPW1PW91[d]	−10.7	−10.2	−8.7	−8.5	−8.3	9.3
BMK[e]	−1.6	−1.2	−0.1	+1.0	−1.1	1.0

[a] NIST: ref 58. CRC: ref 59. Benson: ref 60 + ref 61. [b] CBS-QB3: geometry, frequencies, ZPVE, and partition functions calculated with the B3LYP/6-311G(2d,d,p) level of theory using a scaling factor of 0.99; the electronic energy is assessed using the CBS-QB3 extrapolation scheme. [c] G3B3: geometry, frequencies, ZPVE, and partition functions calculated with the B3LYP/6-31G(d) level of theory using a scaling factor of 0.96; the electronic energy is assessed using the G3B3 extrapolation scheme. [d] MPW1PW91: geometry, frequencies, electronic energy, ZPVE, and partition functions calculated with the MPW1PW91/6-311G(2d,d,p) level of theory using a scaling factor of 0.99. [e] BMK: geometry, frequencies, electronic energy, ZPVE, and partition functions calculated with the B3LYP/6-311G(2d,d,p) level of theory using a scaling factor of 0.99.

TABLE 2: $\langle\rho\rangle$ for a Set Containing Five H Abstractions Calculated with the CBS-QB3, G3B3, MPW1PW91/6-311G(2d,d,p), and BMK/6-311G(2d,d,p) Method at 298, 600, and 1000 K[a]

	$\langle\rho\rangle$ 298 K				$\langle\rho\rangle$ 600 K			
	CBS-QB3[b]	MPW1PW91[c]	G3B3[d]	BMK[e]	CBS-QB3[b]	MPW1PW91[c]	G3B3[d]	BMK[e]
HO	184.6	21.7	2771.1	149.1	5.2	24.2	**7.7**	**6.9**
1D-HR	376.2	***13.5***	5670.7	288.0	5.6	**9.1**	19.7	12.7
1D-HR/W	105.1	33.8	1609.7	78.0	4.7	14.1	12.4	8.6
1D-HR/S&T	37.7	646.1	**23.3**	82.1	4.6	17.1	9.9	7.4
1D-HR/E	**17.6**	164.3	171.4	**17.0**	***4.6***	16.6	10.2	7.5

	$\langle\rho\rangle$ 1000 K				$^1/_3\sum_{T=298,600,1000K}\langle\rho\rangle(T)$			
	CBS-QB3[b]	MPW1PW91[c]	G3B3[d]	BMK[e]	CBS-QB3[b]	MPW1PW91[c]	G3B3[d]	BMK[e]
HO	8.1	28.7	2.6	5.4	66.0	24.9	927.2	53.8
1D-HR	**2.6**	**8.3**	2.6	3.5	128.1	**10.3**	1897.7	101.4
1D-HR/W	3.0	10.0	2.3	3.4	37.6	19.3	541.5	30.0
1D-HR/S&T	3.1	10.3	2.3	**3.3**	15.2	224.5	**11.8**	30.9
1D-HR/E	3.1	10.4	***2.2***	3.3	***8.5***	63.8	61.3	**9.3**

[a] For each level of theory the influence of the 1D-HR approximation and tunneling on $\langle\rho\rangle$ is assessed. Results obtained with the method yielding best agreement with experimental rate coefficients at a certain temperature are Italic and bold for each level of theory. [b] CBS-QB3: geometry, frequencies, ZPVE, and partition functions calculated with the B3LYP/6-311G(2d,d,p) level of theory using a scaling factor of 0.99; the electronic energy is assessed using the CBS-QB3 extrapolation scheme. [c] G3B3: geometry, frequencies, ZPVE, and partition functions calculated with the B3LYP/6-31G(d) level of theory using a scaling factor of 0.96; the electronic energy is assessed using the G3B3 extrapolation scheme. [d] MPW1PW91: geometry, frequencies, electronic energy, ZPVE, and partition functions calculated with the MPW1PW91/6-311G(2d,d,p) level of theory using a scaling factor of 0.99. [e] BMK: geometry, frequencies, electronic energy, ZPVE, and partition functions calculated with the B3LYP/6-311G(2d,d,p) level of theory using a scaling factor of 0.99.

under study. The two selected reaction systems are the H abstraction by methyl from methane and from ethene. The W1 calculations were carried out on B3LYP triple-ζ basis set optimized structures using the MOLPRO computational package.[32] For the abstraction by methyl from methane, W1 calculations yielded a reaction barrier of 73.8 kJ mol^{-1}. The reaction barriers calculated with the CBS-QB3, G3B3, BMK, and MPW1PW91 methods were respectively 71.0, 77.3, 67.7, and 58.9 kJ mol^{-1}. Hence, for this reaction the best result is obtained with the CBS-QB3 method, which slightly underestimates the reaction barrier with 2.8 kJ mol^{-1}. The G3B3 method performs second best, overestimating the reaction barrier with 3.5 kJ mol^{-1}, followed by the BMK theory, which underestimates the barrier for this reaction with 6.1 kJ mol^{-1}. For the abstraction from ethane by methyl, the W1 theory predicts an energy barrier of 78.0 kJ mol^{-1}. This value is best approximated by the G3B3 method which yields a barrier of 75.7 kJ mol^{-1} (see Table 1, reaction **B**). CBS-QB3 underestimates the barrier with almost 9 kJ mol^{-1}, probably caused by spin contamination in the transition state. For this reaction $\langle S^2\rangle$ amounts to 0.95 whereas, for the H abstraction from methane by methyl, spin contamination in the transition state is negligible ($\langle S^2\rangle = 0.79$). Coote[14] also studied the effect of the level of theory on the reaction barriers of H abstractions and reported that for reactions

TABLE 3: Experimental Rate Coefficients at 298, 600 and 1000 K (m^3 mol^{-1} s^{-1})

	Reaction	Reference	k_{exp}		
			298K	600K	1000K
1	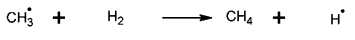	1968WAL		$1.19 \cdot 10^{2}$	$7.12 \cdot 10^{3}$
		1974KOB/PAC		$9.41 \cdot 10^{1}$	$6.46 \cdot 10^{3}$
		1978ART/BEL		$8.81 \cdot 10^{1}$	
		1981MAR/SHA		$7.43 \cdot 10^{1}$	
		1984WAR	$3.63 \cdot 10^{-2}$	$2.15 \cdot 10^{2}$	$1.34 \cdot 10^{4}$
		1986TSA/HAM	$6.27 \cdot 10^{-3}$	$9.10 \cdot 10^{1}$	$8.30 \cdot 10^{3}$
		1988MAN/LOU			$1.35 \cdot 10^{4}$
		1991RAB/SUT		$3.11 \cdot 10^{2}$	$8.37 \cdot 10^{3}$
		1992BAU/COB	$5.11 \cdot 10^{-3}$	$1.04 \cdot 10^{2}$	$9.96 \cdot 10^{3}$
		1996KNY/BEN			$9.64 \cdot 10^{3}$
2		1959DAI/IVI		$3.11 \cdot 10^{0}$	
		1978ART/BEL		$3.28 \cdot 10^{0}$	
3		1972PAC/PUR			$1.02 \cdot 10^{4}$
		1974YAM/RYB			$3.23 \cdot 10^{3}$
		1977HEL/MAN			$3.68 \cdot 10^{2}$
		1978ART/BEL		$3.32 \cdot 10^{1}$	
		1984WAR	$3.64 \cdot 10^{-3}$	$6.84 \cdot 10^{1}$	$8.51 \cdot 10^{3}$
		1986TSA/HAM	$3.63 \cdot 10^{-3}$	$6.82 \cdot 10^{1}$	$8.49 \cdot 10^{3}$
		1992BAU/COB	$3.88 \cdot 10^{-3}$	$4.40 \cdot 10^{1}$	$7.15 \cdot 10^{3}$
4	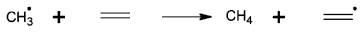	1984WAR	$2.99 \cdot 10^{-3}$	$3.77 \cdot 10^{1}$	$1.57 \cdot 10^{3}$
		1986TSA/HAM	$1.02 \cdot 10^{-3}$	$4.37 \cdot 10^{1}$	$7.00 \cdot 10^{3}$
		1992BAU/COB		$3.68 \cdot 10^{2}$	$1.54 \cdot 10^{4}$
5	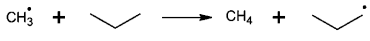	1988TSA	$5.53 \cdot 10^{-3}$	$3 \cdot 10 \cdot 10^{1}$	$2.20 \cdot 10^{3}$
6	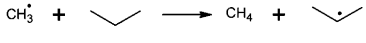	1988TSA	$5.25 \cdot 10^{-2}$	$6.23 \cdot 10^{1}$	$2.29 \cdot 10^{3}$
7	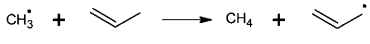	1984WAR		$8.71 \cdot 10^{1}$	
		1987BAL/KEE		$7.95 \cdot 10^{1}$	
		1991TSA	$6.91 \cdot 10^{-2}$	$1.00 \cdot 10^{2}$	$4.02 \cdot 10^{3}$
		1991KIN/ROS	$5.63 \cdot 10^{-2}$	$9.31 \cdot 10^{2}$	
8	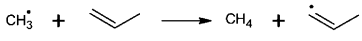	1991TSA	$2.32 \cdot 10^{-7}$	$1.49 \cdot 10^{-1}$	$6.64 \cdot 10^{1}$
9	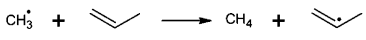	1991TSA	$1.08 \cdot 10^{-6}$	$2.52 \cdot 10^{-1}$	$7.53 \cdot 10^{1}$
10	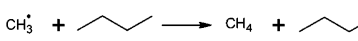	1975YAM			$5.37 \cdot 10^{2}$
11	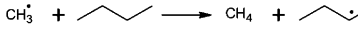	1975YAM			$2.18 \cdot 10^{3}$
12		1990TSA	$8.32 \cdot 10^{-3}$	$4.66 \cdot 10^{1}$	$3.31 \cdot 10^{3}$
		1990ZHA/BAC		$4.63 \cdot 10^{1}$	
13	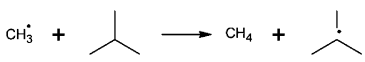	1976YAM/TSI			$5.33 \cdot 10^{3}$
		1990ZHA/BAC		$1.62 \cdot 10^{2}$	
		1990TSA	$1.42 \cdot 10^{-1}$	$7.88 \cdot 10^{1}$	$2.15 \cdot 10^{3}$
14	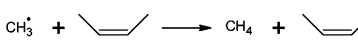	1984WAR	$2.03 \cdot 10^{-1}$	$2.00 \cdot 10^{2}$	

TABLE 3 (Continued)

	Reaction	Reference	k_{exp}		
			298K	600K	1000K
15	$CH_4 + H^{\bullet} \rightarrow CH_3^{\bullet} + H_2$	1964JAM/BRO		$1.22 \cdot 10^{3}$	
		1966LAW/FIR	$1.99 \cdot 10^{1}$		
		1967DIX/WIL		$1.63 \cdot 10^{3}$	$1.11 \cdot 10^{5}$
		1968WAL		$5.82 \cdot 10^{3}$	$3.16 \cdot 10^{5}$
		1970KUR/HOL		$3.70 \cdot 10^{3}$	$1.82 \cdot 10^{5}$
		1971BAK/BAL	$2.32 \cdot 10^{-1}$	$5.73 \cdot 10^{3}$	
		1978SHA	$4.10 \cdot 10^{-1}$	$3.05 \cdot 10^{3}$	$1.65 \cdot 10^{5}$
		1979SEP/MAR		$3.44 \cdot 10^{3}$	$1.88 \cdot 10^{5}$
		1984WAR	$2.26 \cdot 10^{-1}$	$3.11 \cdot 10^{3}$	$2.70 \cdot 10^{5}$
		1986JON/MA	$1.10 \cdot 10^{1}$		
		1986TSA/HAM	$2.22 \cdot 10^{-1}$	$3.11 \cdot 10^{3}$	$2.73 \cdot 10^{5}$
		1991RAB/SUT		$4.22 \cdot 10^{3}$	$1.67 \cdot 10^{5}$
		1992BAU/COB	$4.55 \cdot 10^{-1}$	$3.41 \cdot 10^{3}$	$2.34 \cdot 10^{5}$
		2001BRY/SLA		$1.63 \cdot 10^{3}$	$1.59 \cdot 10^{5}$
		2001SUT/SU		$1.55 \cdot 10^{3}$	$1.47 \cdot 10^{5}$
16	$CH_4 +$ $\rightarrow CH_3^{\bullet} +$	1986TSA/HAM	$9.30 \cdot 10^{-7}$	$7.29 \cdot 10^{-1}$	$4.09 \cdot 10^{2}$
17	$CH_4 +$ $\rightarrow CH_3^{\bullet} +$	1986TSA/HAM	$1.27 \cdot 10^{0}$	$2.19 \cdot 10^{3}$	$1.07 \cdot 10^{5}$
18	$CH_4 +$  $\rightarrow CH_3^{\bullet} +$ 	1988TSA	$2.28 \cdot 10^{-6}$	$3.90 \cdot 10^{-1}$	$1.17 \cdot 10^{2}$
19	$CH_4 +$  $\rightarrow CH_3^{\bullet} +$ 	1988TSA	$6.81 \cdot 10^{-7}$	$1.42 \cdot 10^{-1}$	$5.03 \cdot 10^{1}$
20	$CH_4 +$  $\rightarrow CH_3^{\bullet} +$ 	1990TSA	$4.77 \cdot 10^{-5}$	$5.71 \cdot 10^{-1}$	$5.56 \cdot 10^{1}$
21	$CH_4 +$  $\rightarrow CH_3^{\bullet} +$ 	1990TSA	$1.83 \cdot 10^{-8}$	$1.99 \cdot 10^{-2}$	$1.69 \cdot 10^{1}$

where spin contamination is observed, the Gaussian-3 methods reproduce more accurately the reaction barriers than CBS-QB3. The authors attributed the errors in the calculated CBS-QB3 barriers to the empirical spin-correction term used in CBS-QB3.[14] Despite the problems with spin contamination, the CBS-QB3 method provides the best agreement with experimental rate coefficients for the set of five reactions. Therefore, this method was selected to perform a more detailed study on the influence of the 1D hindered rotor treatment and tunneling on the rate coefficients of hydrogen abstractions.

3.2. Harmonic Oscillator Approximation vs 1D-HR Treatment. Rate coefficients for hydrogen abstractions between hydrocarbons were taken from the NIST Chemical Kinetics Database at $T = 298$, 600, and 1000 K.[28] Experimental data were retrieved for 21 reactions all involving the abstraction of a hydrogen atom from a hydrocarbon by methyl or from methane by an alkyl radical (Table 3). For all these reactions the internal rotation about the forming/breaking C−H−C bond in the transition state has a symmetry number of 3. The potential energy surface for the rotation about this transition state bond can hence be considered as

$$V(\theta) = V_{\max}\frac{(1 - \cos 3\theta)}{2} \qquad (25)$$

In eq 25 V_{max} is the maximal potential energy rise when both interacting fragments of the transition state move from anti to eclipse conformation. As the average distance between the two fragments is large, typically around 260−280 pm, the average V_{max} for the test set is small and ranges from 0.2 to 0.35 kJ mol^{-1} (see Table S1 of the Supporting Information). If $V_{max} \ll RT$ the rotation can be considered in good approximation as a free rotor. This is illustrated in Figure 1 where the influence of the 1D-HR and 1D free rotor (1D-FR) treatment on the partition function q for the rotation about the transition state bond are compared at 200 and 1100 K, assuming that the potential energy profile for rotation is given in good approximation by eq 25. In the potential energy interval of interest (0.2−0.35 kJ mol^{-1}) the ratio q_{HO}/q_{1D-HR} varies between 3 and 10. As rotational barriers are low, at high temperatures both the 1D hindered rotor and 1D free rotor partition functions coincide. Obviously for the hydrogen abstractions of the database accurate kinetic data can be obtained within the 1D-FR treatment. However, as in other H abstractions between hydrocarbons the rotational barrier amounts to values larger than 1 kJ mol^{-1}, the 1D-HR approach will be systematically applied. For example, for the abstraction from a secondary hydrogen atom of propane by 1-propyl V_{max} equals 2.1 kJ mol^{-1} and the 1D-HR and 1D-FR calculated rate coefficients differ almost by a factor 2 at 200 K.

In Figure 2 the influence of the 1D-HR treatment on the Arrhenius parameters is illustrated for $V_{max} = 0.1$, 0.3, and 0.5 kJ mol^{-1} at different temperatures in the interval 300−1000 K. The influence of the 1D hindered rotor treatment on the activation energy ($\Delta E_a = E_{a,1D-HR} - E_{a,HO}$) and on the pre-exponential factor ($\Delta \log A = \log A_{1D-HR} - \log A_{HO}$) are shown

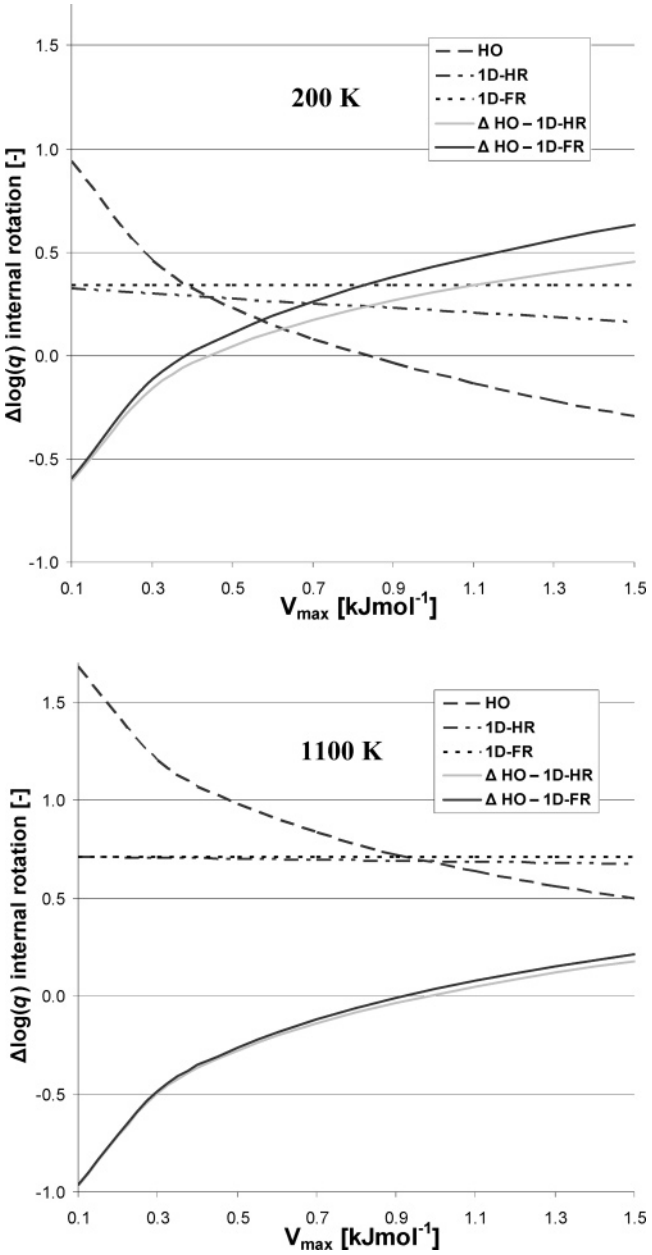

Figure 1. Influence of the 1D-HR and 1D-FR approximation on the molar partition function for internal rotation about the forming/breaking C−H−C bond of the transition state.

along respectively the ordinate and the abscissa at temperatures ranging from 300 to 1000 K and for rotational barriers V_{max} ranging from 0.1 to 0.5 kJ mol^{-1}. Figure 2 illustrates that both the activation energy E_a and pre-exponential factor A decrease when the rotation about the transition state C−H−C bond is modeled as a hindered rotor. Figure 2 also shows that the absolute magnitude of the 1D-HR corrections on both Arrhenius parameters increase with increasing temperature and decreases with increasing rotational barrier. Both temperature and rotational hindrance have a pronounced effect on log A. In contrast to log A, ΔE_a is almost independent of rotational hindrance and varies from −1.1 kJ mol^{-1} at 300 K to −4.1 kJ mol^{-1} at 1000 K. The decrease in E_a corresponds on average to an increase of the rate coefficient with a factor 1.6. A larger impact on the rate coefficient stems from changes in log A. The decrease in log A amounts to temperature averaged values of 1.1, 0.6, and 0.4 for rotational barriers of respectively 0.1, 0.3, and 0.5 kJ mol^{-1}. This decrease in log A corresponds to a decrease in the rate coefficient k with respectively a factor 12.6, 4.0, and 2.5.

Rate coefficients were calculated within the HO and 1D-HR approximation for a large experimental database consisting of 21 hydrogen abstractions reactions (Table 3). The results are shown in Table 4. The 1D-HR approximation on average lowers the rate coefficients of the set of reactions with a factor of 1.8 at 298 K, 2.5 at 600 K, and 3.2 at 1000 K. The necessity for the 1D-HR rotor treatment for the internal rotation about the breaking/forming bond of the TS is confirmed by the low HO frequencies calculated for this mode. For the 21 reactions of the data base it was found that the frequencies for this internal rotation ranged from 12 to 46 cm^{-1} (see Table S1 of the Supporting Information).

An overall compilation of the theoretical HO and 1D-HR data is given in Table 5. At lower temperatures the HO treatment yields better agreement with experiment than the 1D-HR method. At 298 K $\langle\rho\rangle$ equals 123 within the HO approximation and almost doubles within the 1D-HR treatment. At low temperatures, nonclassical low-energy reactions will contribute in large part to the measured rate coefficient but are not accounted for in the classical transition state theory. Due to this neglect of tunneling, the ab initio rate coefficients are systematically underestimated. As 1D-HR corrections decrease the rate coefficients, the deviation from experiment becomes even more pronounced. At high temperatures, rate coefficients calculated with CTST are systematically overestimated due to recrossing effects. As a maximum in potential energy along the reaction path does not necessarily correspond with a maximum in the Gibbs free energy, the reactants can cross the transition state without reacting. This leads to CTST rate coefficients that are systematically overestimated. As 1D-HR causes rate coefficients to decrease, accounting for hindered rotations improves the agreement with experiment, as evidenced by the reduction of $\langle\rho\rangle$ from 7.2 within the HO approximation to 3.2 within the 1D-HR treatment at 1000 K.

3.3. Tunneling. One of the drawbacks of conventional transition state theory is that it does not account for quantum effects such as tunneling. In the previous paragraph it was mentioned that the theoretically more accurate 1D-HR treatment did not yield better agreement with the experimental rate coefficients than the HO approximation. At lower temperatures the neglect of tunneling contributions leads to large deviations between the 1D-HR and experimental rate coefficients. Therefore the influence of tunneling on the rate coefficient will be studied in more detail. First the zero curvature tunneling methods are compared with the more advanced centrifugal dominant small curvature tunneling method. Finally, rate coefficients calculated within the 1D-HR approximation with tunneling corrections are compared with experimental data obtained from the NIST Chemical Kinetics Database. In Figure 3 transmission coefficients are plotted for the abstraction of a hydrogen atom from methane by methyl in the temperature range 300−800 K for the four different tunneling methodologies presented in section 3. The CD-SCS transmission coefficients are validated by comparison with the equivalent small-curvature-approximation semiclassical adiabatic ground state (CSCAG) transmission coefficients reported by Kungwan and Truong.[56] Both CD-SCS and CSCAG are in excellent agreement at higher temperatures; at temperatures below 500 K small deviations are observed between our values and those reported by Kungwan and Truong. The small deviation is probably due to a different integration grid and integration procedure along the reaction path. At high temperatures all tunneling corrections are in fairly good agree-

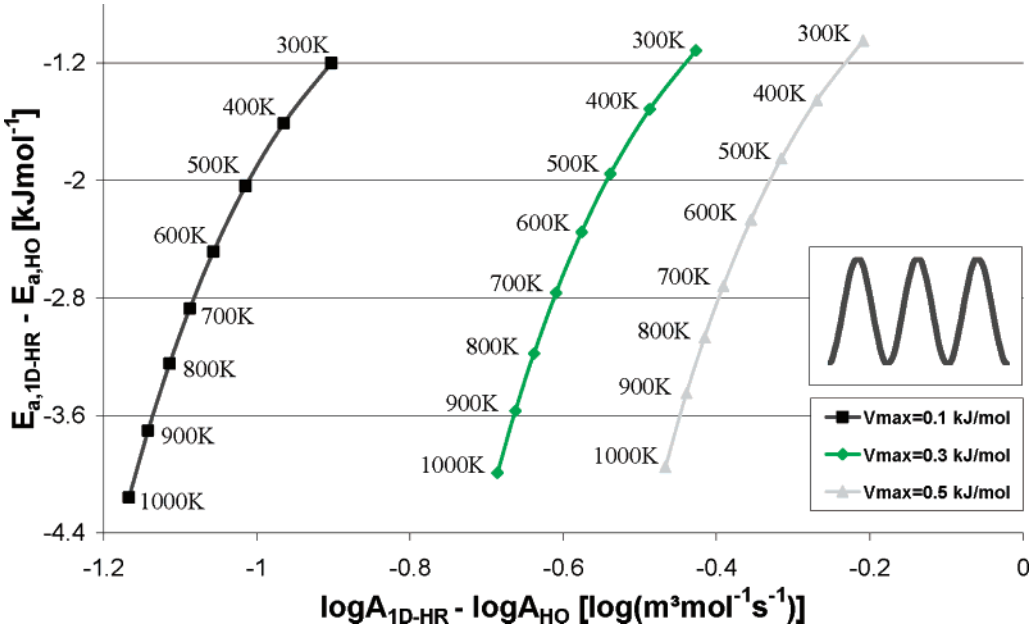

Figure 2. Influence of the 1D-HR approximation on the Arrhenius parameters in the temperature interval 300−1000 K.

ment. At lower temperatures (<500 K) the tunneling correction proposed by Wigner underestimates tunneling contributions significantly, but on the other hand, the S&T tunneling correction overestimates tunneling contributions when temperatures fall below 400 K. Best agreement with the CD-SCS tunneling coefficients is obtained with the Eckart tunneling correction and accurate tunneling corrections can be obtained for temperatures far below 300 K. For example at 200 K $\kappa_{S\&T} = 1.05 \times 10^9$ whereas the more accurate CD-SCS method predicts a tunneling correction of 1.94×10^5. The Skodje and Truhlar formula hence largely overestimates tunneling contributions up to a factor of 10^4 at these low temperatures. The Eckart methods predicts $\kappa_{Eckart} = 1.62 \times 10^5$ at 200 K, which is in remarkably good agreement with the CD-SCS value.

In Figures 4 and 5 experimental rate coefficients are compared with ab initio calculated rate coefficients for two hydrogen abstraction reactions for which multiple consistent kinetic data were available in the NIST Chemical Kinetics Database.[28] The two studied reactions are

(**1**) $CH_3^\bullet + CH_4 \rightarrow CH_4 + C^\bullet H_3$ (Figure 4)

(**2**) $CH_3^\bullet + C_2H_6 \rightarrow CH_4 + C_2^\bullet H_5$ (Figure 5)

For both reactions good agreement between the experimental data and ab initio calculated rate coefficients was obtained. As seen from Figures 4 and 5 the best agreement between experimental and ab initio rate coefficients for reactions 1 and 2 is found respectively with the 1D-HR/CD-SCS and the 1D-HR/Eckart method. For reaction 2 (Figure 5), the theoretically more accurate CD-SCS method seems to overestimate tunneling contributions. This is probably due to recrossing effects. For reaction 1, i.e., the symmetric hydrogen abstraction from methane by methyl, it was found that the variational and classical transition state coincide. Hence for this reaction no recrossing effects take place and therefore better agreement with the experimental rate coefficients is obtained with the 1D-HR/CD-SCS approach. Figure 5 illustrates once more that at temperatures below 400 K the zero curvature tunneling method of Skodje and Truhlar tends to overestimate tunneling contributions.

From Figures 4 and 5 it can also be seen that the 1D hindered rotor corrected tunneling methods perform well in describing the temperature dependence of the rate coefficient as the calculated curves succeed to follow the experimental data over a large temperature interval. As shown in Figure 3, the Eckart method slightly underestimates tunneling corrections at 300−800 K due to the neglect of corner cutting effects. However, this effect is partially neutralized by the inclusion of recrossing effects in the CTST rate coefficients. Hence for reaction 2 the conventional 1D-HR approach with tunneling corrections as proposed by Eckart yield results that are even better than those obtained with the computationally more demanding 1D-HR/CD-SCS methodology.

Rate coefficients for all 21 reactions were calculated within the three ZCT corrected 1D-HR approaches (1D-HR/W, 1D-HR/S&T, and 1D-HR/E) and compared to the experimental data of Table 3. The calculated 1D-HR/W, 1D-HR/S&T, and 1D-HR/E rate coefficients are shown in Table 4. The values of $\langle\rho\rangle$ at 298, 600, and 1000 K are reported in Table 5.

It is seen from Table 5 that tunneling corrections drastically improve results at 298 K, lowering $\langle\rho\rangle$ from 225 to 64 for Wigner, to 17 for S&T, and to 10 for Eckart. As tunneling coefficients are dependent on the imaginary frequency, some of the remaining deviations with experiment can be caused by faulty imaginary frequencies obtained with the B3LYP functional. Coote[57] reported that for H abstractions scaling of the B3LYP triple-ζ basis set, imaginary frequencies by a factor of 1.15 led to better agreement with high-level CCSD(T) imaginary frequencies. However, for the set of 21 reactions, scaling the imaginary frequencies with 1.15 did not significantly improve the agreement of the calculated rate coefficients with experiment at 298 K. For example within the Eckart tunneling scheme scaling of the imaginary frequencies decreased $\langle\rho\rangle$ only from 10.0 to 9.7. Hence no additional scaling factor for the imaginary frequencies was used in this work. At 600 K the inclusion of tunneling leads to slightly better results than obtained with the non tunneling corrected 1D-HR approach. As tunneling contributions are limited to a factor 2.2 at this temperature, the effect is less pronounced than at 298 K. $\langle\rho\rangle$ fluctuates between values of 3.9 for 1D-HR/E and 5.0 for the non tunneling corrected 1D-HR treatment. At 1000 K best performance is even

TABLE 4: Calculated CBS-QB3[a] Rate Coefficients at 298, 600, and 1000 K (m^3 mol^{-1} s^{-1}) for the Reactions in Table 3

	Reaction	T	k_{calc}				
			HO	1D-HR	1D-HR/W	1D-HR/S&T	1D-HR/E
1	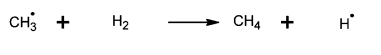	298K	$4.94 \cdot 10^{-4}$	$4.94 \cdot 10^{-4}$	$1.05 \cdot 10^{-3}$	$2.50 \cdot 10^{-3}$	$1.95 \cdot 10^{-3}$
		600K	$4.14 \cdot 10^{1}$	$4.14 \cdot 10^{1}$	$5.29 \cdot 10^{1}$	$5.56 \cdot 10^{1}$	$5.62 \cdot 10^{1}$
		1000K	$4.79 \cdot 10^{3}$	$4.79 \cdot 10^{3}$	$5.25 \cdot 10^{3}$	$5.28 \cdot 10^{3}$	$5.34 \cdot 10^{3}$
2	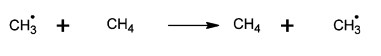	298K	x	x	x	x	x
		600K	$2.48 \cdot 10^{0}$	$1.05 \cdot 10^{0}$	$1.74 \cdot 10^{0}$	$2.26 \cdot 10^{0}$	$2.17 \cdot 10^{0}$
		1000K	x	x	x	x	x
3	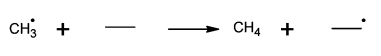	298K	$2.51 \cdot 10^{-4}$	$1.45 \cdot 10^{-4}$	$5.08 \cdot 10^{-4}$	$6.92 \cdot 10^{-2}$	$5.39 \cdot 10^{-3}$
		600K	$8.49 \cdot 10^{1}$	$3.55 \cdot 10^{1}$	$5.74 \cdot 10^{1}$	$7.29 \cdot 10^{1}$	$7.06 \cdot 10^{1}$
		1000K	$2.66 \cdot 10^{4}$	$8.72 \cdot 10^{3}$	$1.06 \cdot 10^{4}$	$1.09 \cdot 10^{4}$	$1.11 \cdot 10^{4}$
4	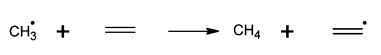	298K	$2.55 \cdot 10^{-6}$	$1.22 \cdot 10^{-6}$	$4.42 \cdot 10^{-6}$	$2.97 \cdot 10^{-4}$	$4.02 \cdot 10^{-5}$
		600K	$7.28 \cdot 10^{0}$	$2.51 \cdot 10^{0}$	$4.12 \cdot 10^{0}$	$5.33 \cdot 10^{0}$	$5.10 \cdot 10^{0}$
		1000K	$5.27 \cdot 10^{3}$	$1.42 \cdot 10^{3}$	$1.77 \cdot 10^{3}$	$1.84 \cdot 10^{3}$	$1.87 \cdot 10^{3}$
5	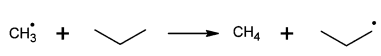	298K	$4.82 \cdot 10^{-5}$	$2.68 \cdot 10^{-5}$	$9.57 \cdot 10^{-5}$	$1.44 \cdot 10^{-2}$	$1.07 \cdot 10^{-3}$
		600K	$1.40 \cdot 10^{1}$	$5.63 \cdot 10^{0}$	$9.20 \cdot 10^{0}$	$1.18 \cdot 10^{1}$	$1.14 \cdot 10^{1}$
		1000K	$4.13 \cdot 10^{3}$	$1.30 \cdot 10^{3}$	$1.59 \cdot 10^{3}$	$1.65 \cdot 10^{3}$	$1.67 \cdot 10^{3}$
6	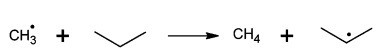	298K	$8.26 \cdot 10^{-3}$	$4.71 \cdot 10^{-3}$	$1.58 \cdot 10^{-2}$	$6.84 \cdot 10^{-1}$	$1.13 \cdot 10^{-1}$
		600K	$3.92 \cdot 10^{2}$	$1.62 \cdot 10^{2}$	$2.56 \cdot 10^{2}$	$3.17 \cdot 10^{2}$	$3.08 \cdot 10^{2}$
		1000K	$5.71 \cdot 10^{4}$	$1.85 \cdot 10^{4}$	$2.23 \cdot 10^{4}$	$2.29 \cdot 10^{4}$	$2.32 \cdot 10^{4}$
7	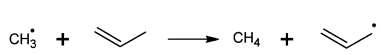	298K	$2.69 \cdot 10^{-2}$	$1.52 \cdot 10^{-2}$	$4.80 \cdot 10^{-2}$	$9.69 \cdot 10^{-1}$	$2.48 \cdot 10^{-1}$
		600K	$3.54 \cdot 10^{2}$	$1.44 \cdot 10^{2}$	$2.22 \cdot 10^{2}$	$2.64 \cdot 10^{2}$	$2.57 \cdot 10^{2}$
		1000K	$3.07 \cdot 10^{4}$	$9.83 \cdot 10^{3}$	$1.17 \cdot 10^{4}$	$1.20 \cdot 10^{4}$	$1.21 \cdot 10^{4}$
8	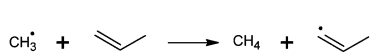	298K	$5.65 \cdot 10^{-7}$	$2.80 \cdot 10^{-7}$	$9.52 \cdot 10^{-7}$	$3.36 \cdot 10^{-5}$	$6.36 \cdot 10^{-6}$
		600K	$1.95 \cdot 10^{0}$	$6.96 \cdot 10^{-1}$	$1.11 \cdot 10^{0}$	$1.38 \cdot 10^{0}$	$1.33 \cdot 10^{0}$
		1000K	$1.52 \cdot 10^{3}$	$4.22 \cdot 10^{2}$	$5.12 \cdot 10^{2}$	$5.28 \cdot 10^{2}$	$5.37 \cdot 10^{2}$
9	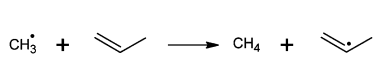	298K	$3.57 \cdot 10^{-5}$	$1.95 \cdot 10^{-5}$	$6.93 \cdot 10^{-5}$	$5.32 \cdot 10^{-3}$	$5.92 \cdot 10^{-4}$
		600K	$1.58 \cdot 10^{1}$	$6.25 \cdot 10^{0}$	$1.02 \cdot 10^{1}$	$1.30 \cdot 10^{1}$	$1.25 \cdot 10^{1}$
		1000K	$5.50 \cdot 10^{3}$	$1.70 \cdot 10^{3}$	$2.09 \cdot 10^{3}$	$2.16 \cdot 10^{3}$	$2.20 \cdot 10^{3}$
10	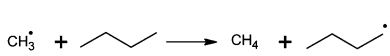	298K	x	x	x	x	x
		600K	x	x	x	x	x
		1000K	$5.68 \cdot 10^{3}$	$1.73 \cdot 10^{3}$	$2.12 \cdot 10^{3}$	$2.20 \cdot 10^{3}$	$2.23 \cdot 10^{3}$
11	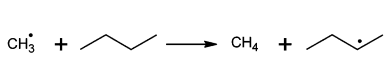	298K	x	x	x	x	x
		600K	x	x	x	x	x
		1000K	$1.64 \cdot 10^{4}$	$4.86 \cdot 10^{3}$	$5.87 \cdot 10^{3}$	$6.05 \cdot 10^{3}$	$6.13 \cdot 10^{3}$
12		298K	$6.81 \cdot 10^{-5}$	$4.15 \cdot 10^{-5}$	$1.49 \cdot 10^{-4}$	$2.31 \cdot 10^{-2}$	$1.68 \cdot 10^{-3}$
		600K	$2.04 \cdot 10^{1}$	$9.04 \cdot 10^{0}$	$1.48 \cdot 10^{1}$	$1.91 \cdot 10^{1}$	$1.84 \cdot 10^{1}$
		1000K	$6.08 \cdot 10^{3}$	$2.12 \cdot 10^{3}$	$2.60 \cdot 10^{3}$	$2.70 \cdot 10^{3}$	$2.74 \cdot 10^{3}$
13		298K	$8.73 \cdot 10^{-2}$	$5.04 \cdot 10^{-2}$	$1.57 \cdot 10^{-1}$	$2.26 \cdot 10^{0}$	$6.95 \cdot 10^{-1}$
		600K	$6.31 \cdot 10^{2}$	$2.65 \cdot 10^{2}$	$4.03 \cdot 10^{2}$	$4.78 \cdot 10^{2}$	$4.68 \cdot 10^{2}$
		1000K	$4.41 \cdot 10^{4}$	$1.45 \cdot 10^{4}$	$1.72 \cdot 10^{4}$	$1.76 \cdot 10^{4}$	$1.77 \cdot 10^{4}$
14		298K	$4.64 \cdot 10^{-2}$	$2.89 \cdot 10^{-2}$	$8.77 \cdot 10^{-2}$	$1.22 \cdot 10^{0}$	$3.76 \cdot 10^{-1}$
		600K	$3.95 \cdot 10^{2}$	$1.36 \cdot 10^{2}$	$2.66 \cdot 10^{2}$	$3.11 \cdot 10^{2}$	$3.03 \cdot 10^{2}$
		1000K	x	x	x	x	x

TABLE 4 (Continued)

	Reaction	T	k_{calc}				
			HO	1D-HR	1D-HR/W	1D-HR/S&T	1D-HR/E
15	$CH_4 + H^{\bullet} \rightarrow CH_3^{\bullet} + H_2$	298K	$8.44 \cdot 10^{-3}$	$8.44 \cdot 10^{-3}$	$1.80 \cdot 10^{-2}$	$4.27 \cdot 10^{-2}$	$3.33 \cdot 10^{-2}$
		600K	$2.87 \cdot 10^{3}$	$2.87 \cdot 10^{3}$	$3.67 \cdot 10^{3}$	$3.86 \cdot 10^{3}$	$3.90 \cdot 10^{3}$
		1000K	$4.34 \cdot 10^{5}$	$4.34 \cdot 10^{5}$	$4.78 \cdot 10^{5}$	$4.81 \cdot 10^{5}$	$4.86 \cdot 10^{5}$
16	$CH_4 +$	298K	$4.17 \cdot 10^{-8}$	$2.40 \cdot 10^{-8}$	$8.43 \cdot 10^{-8}$	$1.15 \cdot 10^{-5}$	$8.94 \cdot 10^{-7}$
		600K	$3.30 \cdot 10^{-1}$	$1.38 \cdot 10^{-1}$	$2.24 \cdot 10^{-1}$	$2.84 \cdot 10^{-1}$	$2.75 \cdot 10^{-1}$
		1000K	$3.66 \cdot 10^{2}$	$1.20 \cdot 10^{2}$	$1.46 \cdot 10^{2}$	$1.50 \cdot 10^{2}$	$1.53 \cdot 10^{2}$
17	$CH_4 +$	298K	$8.13 \cdot 10^{-3}$	$3.90 \cdot 10^{-3}$	$1.41 \cdot 10^{-2}$	$9.46 \cdot 10^{-1}$	$1.28 \cdot 10^{-1}$
		600K	$3.00 \cdot 10^{2}$	$1.03 \cdot 10^{2}$	$1.70 \cdot 10^{2}$	$2.20 \cdot 10^{2}$	$2.11 \cdot 10^{2}$
		1000K	$4.23 \cdot 10^{4}$	$1.14 \cdot 10^{4}$	$1.42 \cdot 10^{4}$	$1.48 \cdot 10^{4}$	$1.50 \cdot 10^{4}$
18	$CH_4 +$	298K	$4.54 \cdot 10^{-8}$	$2.52 \cdot 10^{-8}$	$9.01 \cdot 10^{-8}$	$1.36 \cdot 10^{-5}$	$1.01 \cdot 10^{-6}$
		600K	$2.47 \cdot 10^{-1}$	$9.94 \cdot 10^{-2}$	$1.63 \cdot 10^{-1}$	$2.09 \cdot 10^{-1}$	$2.01 \cdot 10^{-1}$
		1000K	$2.36 \cdot 10^{2}$	$7.44 \cdot 10^{1}$	$9.13 \cdot 10^{1}$	$9.44 \cdot 10^{1}$	$9.59 \cdot 10^{1}$
19	$CH_4 +$	298K	$2.02 \cdot 10^{-8}$	$1.15 \cdot 10^{-8}$	$3.87 \cdot 10^{-8}$	$1.67 \cdot 10^{-6}$	$2.76 \cdot 10^{-7}$
		600K	$2.42 \cdot 10^{-1}$	$9.99 \cdot 10^{-2}$	$1.58 \cdot 10^{-1}$	$1.95 \cdot 10^{-1}$	$1.90 \cdot 10^{-1}$
		1000K	$3.26 \cdot 10^{2}$	$1.05 \cdot 10^{2}$	$1.27 \cdot 10^{2}$	$1.31 \cdot 10^{2}$	$1.33 \cdot 10^{2}$
20	$CH_4 +$	298K	$6.83 \cdot 10^{-8}$	$4.16 \cdot 10^{-8}$	$1.49 \cdot 10^{-7}$	$2.31 \cdot 10^{-5}$	$1.69 \cdot 10^{-6}$
		600K	$2.88 \cdot 10^{-1}$	$1.28 \cdot 10^{-1}$	$2.10 \cdot 10^{-1}$	$2.70 \cdot 10^{-1}$	$2.60 \cdot 10^{-1}$
		1000K	$2.50 \cdot 10^{2}$	$8.72 \cdot 10^{1}$	$1.07 \cdot 10^{2}$	$1.11 \cdot 10^{2}$	$1.13 \cdot 10^{2}$
21	$CH_4 +$	298K	$1.60 \cdot 10^{-8}$	$9.26 \cdot 10^{-9}$	$2.89 \cdot 10^{-8}$	$4.14 \cdot 10^{-7}$	$1.28 \cdot 10^{-7}$
		600K	$1.36 \cdot 10^{-1}$	$5.68 \cdot 10^{-2}$	$8.65 \cdot 10^{-2}$	$1.03 \cdot 10^{-1}$	$1.00 \cdot 10^{-1}$
		1000K	$1.69 \cdot 10^{2}$	$5.56 \cdot 10^{1}$	$6.61 \cdot 10^{1}$	$6.76 \cdot 10^{1}$	$6.87 \cdot 10^{1}$

[a] CBS-QB3: geometry, frequencies, ZPVE, and partition functions calculated with the B3LYP/6-311G(2d,d,p) level of theory using a scaling factor of 0.99; the electronic energy is assessed using the CBS-QB3 extrapolation scheme. x = no experimental data available.

TABLE 5: Average Ratio of the CBS-QB3[a] Calculated and Experimental Rate Coefficients $\langle\rho\rangle$[b] at 298, 600, and 1000 K for the Reactions in Table 3

T, K	HO	1D-HR	1D-HR/W	1D-HR/S&T	1D-HR/E
298	122.8	225.4	63.8	16.9	10.0
600	4.2	5.0	4.0	3.9	3.9
1000	7.2	3.4	3.6	3.6	3.6
$^1/_3\sum_{T=298,600,1000K}\langle\rho\rangle(T)$	44.7	77.9	23.6	8.1	5.8

[a] CBS-QB3: geometry, frequencies, ZPVE, and partition functions calculated with the B3LYP/6-311G(2d,d,p) level of theory using a scaling factor of 0.99; the electronic energy is assessed using the CBS-QB3 extrapolation scheme [b] Rate coefficients according to Baulch et al. for reaction **4** and according to Tsang et al. for reaction **9** are not included in the calculation of the uncertainty factor $\langle\rho\rangle$. For these reactions the authors proposed a correlation that was not experimentally verified and led to large deviations between all ab initio and experimental rate coefficients.

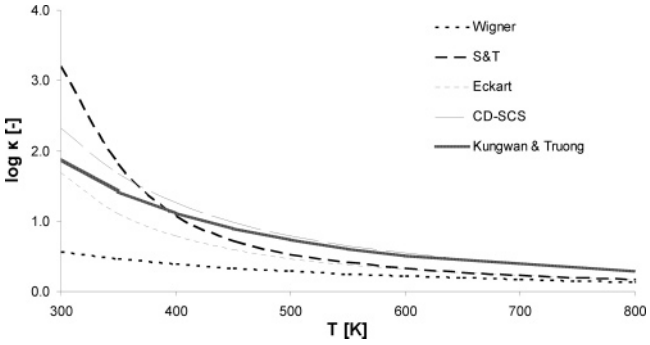

Figure 3. Transmission coefficients for the H abstraction from methane by methyl at 300−800 K according to the ZCT methodologies of Wigner, S&T, and Eckart and the CD-SCS tunneling method.

obtained with the 1D-HR approach. For this method $\langle\rho\rangle$ equals 3.4, which is slightly smaller than the $\langle\rho\rangle$ obtained with the tunneling corrected 1D-HR methodologies. As the 1D-HR rate coefficients are systematically too high due to recrossing effects and as tunneling coefficients $\kappa(T) > 1$, correcting the 1D-HR rate coefficient for tunneling at 1000 K will yield less good agreement between experimental and calculated rate coefficients. Arithmetic mean $\langle\rho\rangle$ values over the three studied temperatures can also be found at the bottom of Table 5. As a measure for the total accuracy of a theoretical method over the entire temperature interval, uncertainty factors are defined as twice $\langle\rho\rangle$. From Table 5 it is seen that the 1D-HR/E approach yields the best result over the entire temperature interval with an average $\langle\rho\rangle$ of 5.8 corresponding to an uncertainty factor of 11.6. The non tunneling corrected ab initio methods perform poorly as $\langle\rho\rangle$ rises up to 78. This is mainly due to disappointing results obtained at low temperatures. Summarizing: tunneling corrections play a critical role in obtaining accurate rate coefficients for H abstractions and this especially at lower temperatures,

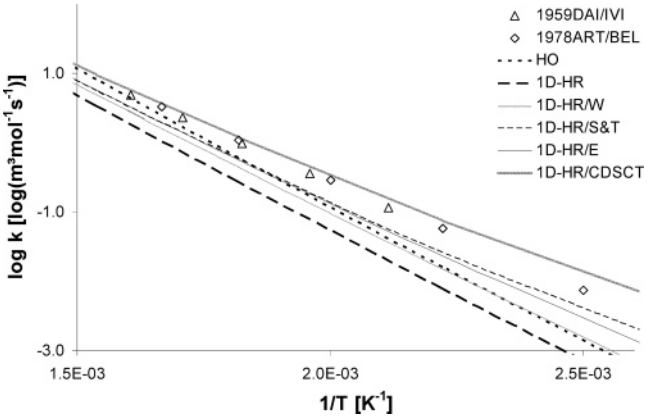

Figure 4. Comparison of ab initio and experimental rate coefficients for the H abstraction from methane by methyl.

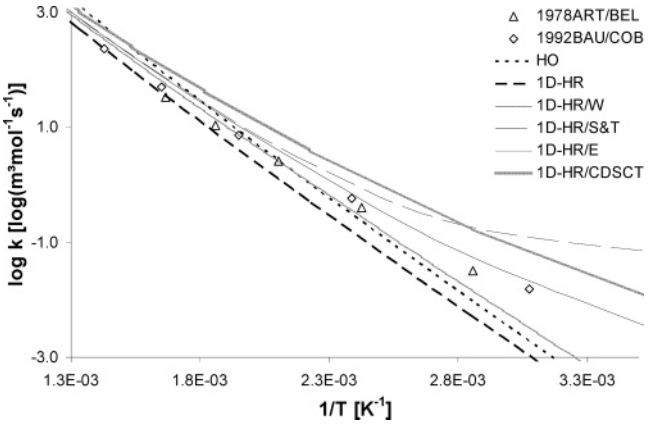

Figure 5. Comparison of ab initio and experimental rate coefficients for the H abstraction from ethane by methyl.

whereas the hindered rotor treatment only contributes to better experimental agreement in the high-temperature range.

3.4. Arrhenius Parameters. In Figure 6 the HO, 1D-HR, and 1D-HR/E activation energies and pre-exponential factors at 298 K are presented for those reactions of Table 3 for which experimental data at 298 K are available. Numerical values for the HO, 1D-HR, 1D-HR/W, 1D-HR/S&T, and 1D-HR/E E_a and log A for all reactions at 298, 600, and 1000 K can be found in Tables S2 and S3 of the Supporting Information.

For the set of reactions, HO activation energies at 298 K range from 40 to 77 kJ mol^{-1} (Figure 6A). The activation energies are temperature dependent and increase approximately by 7 kJ mol^{-1} at 600 K and 18 kJ mol^{-1} at 1000 K. The effect of the 1D-HR on E_a at 298 K is limited to 1 kJ mol^{-1}. However, the influence of the 1D hindered rotor treatment on E_a gains importance when temperatures increase. At 600 K E_a can decrease up to 2.3 kJ mol^{-1} and up to 4.3 kJ mol^{-1} at 1000 K. It can be seen from Figure 6A that tunneling contributions have a more pronounced effect on E_a. With the Eckart tunneling scheme ΔE_a at 298 K can decrease up to 35 kJ mol^{-1}. It was found that the decrease in E_a depends on the barrier height/width of the reaction, tunneling method, and temperature. As expected, the effect of tunneling on the activation energy decreases with increasing temperature. At 600 and 1000 K the Eckart method on average lowers E_a with respectively 8 and 4 kJ mol^{-1}.

From Figure 6B it is seen that at 298 K log A ranges from 8.4 to 10.7. As for E_a, log A increases with increasing temperature. Figure 6B illustrates that the average decrease in log A due to the 1D-HR treatment amounts to 0.4 at 298 K. At low temperatures tunneling contributions tend to have a large impact on log A. At 298 K log A can decrease up to 3 orders of magnitude within the Eckart scheme (Figure 6B). As temperatures increase, the effect of tunneling contributions on log A diminishes rapidly. At 1000 K this effect is almost negligible, as Δ log A is limited to -0.11.

4. Conclusions

A level of theory study was performed for the thermodynamics and kinetics of H abstractions between methyl radicals and simple hydrocarbons or H_2. A comparative study on a set consisting of five hydrogen abstraction reactions showed that the best agreement with experimental rate coefficients was obtained with the CBS-QB3 method. The BMK functional yields results that are close to those obtained with the CBS-QB3 method, indicating that this functional is an attractive low-cost tool to study the considered hydrogen abstraction. The G3B3 method and the MPW1PW91 functional perform rather poorly for this set of five H-abstraction reactions, respectively underestimating and overestimating rate coefficients significantly. The calculated reaction barriers were validated by comparison with high-level Weizmann-1 calculations. This indicated that most accurate reaction barriers are obtained with the composite methods: CBS-QB3 predicts most accurate barriers for reactions where no spin contamination is observed in the transition state, whereas G3B3 outperforms the CBS-QB3 method in yielding accurate barriers for spin-contaminated systems.

The influence of the 1D hindered internal rotation treatment about the forming/breaking bond of the TS and the treatment of quantum effects was assessed at the CBS-QB3 level. At 1000 K modeling of the internal rotation about the TS bond as a 1D hindered rotation improved the agreement between experimental and ab initio data. At lower temperatures the 1D-HR approximation did not yield better results mainly due to the neglect of quantum effects.

For the H abstraction from methane by methyl, accurate tunneling coefficients can be obtained with the advanced CD-SCS method. However, this tunneling method is rather computationally demanding and does not always succeed in predicting accurate rate coefficients, especially for reactions where recrossing effects are likely to occur. Alternatively, three zero curvature tunneling methods were studied (Wigner, Skodje & Truhlar, and Eckart). Especially at low temperatures tunneling contributions have a much more pronounced effect on the rate coefficient of H abstractions than 1D-HR corrections and increase rate coefficients remarkably. The most accurate rate coefficients for hydrogen abstractions were obtained using CBS-QB3 with corrections for the 1D hindered internal rotation about the TS-bond and inclusion of Eckart tunneling contributions.

Acknowledgment. This work is supported by the Fund for Scientific Research Flanders (FWO) and the Institute for Science and Technology (IWT). J. M. L. Martin is acknowledged for technical support with the MOLPRO package.

Appendix A: The Eckart Potential[50]

In the Eckart tunneling correction methodology the potential energy profile is approximated by a function of the form

$$V(s) = \frac{a e^{\alpha(s-s_o)}}{1 + e^{\alpha(s-s_o)}} + \frac{b e^{\alpha(s-s_o)}}{(1 + e^{\alpha(s-s_o)})^2} + c \qquad (26)$$

where s is the reaction coordinate. The parameters a, b, c, α,

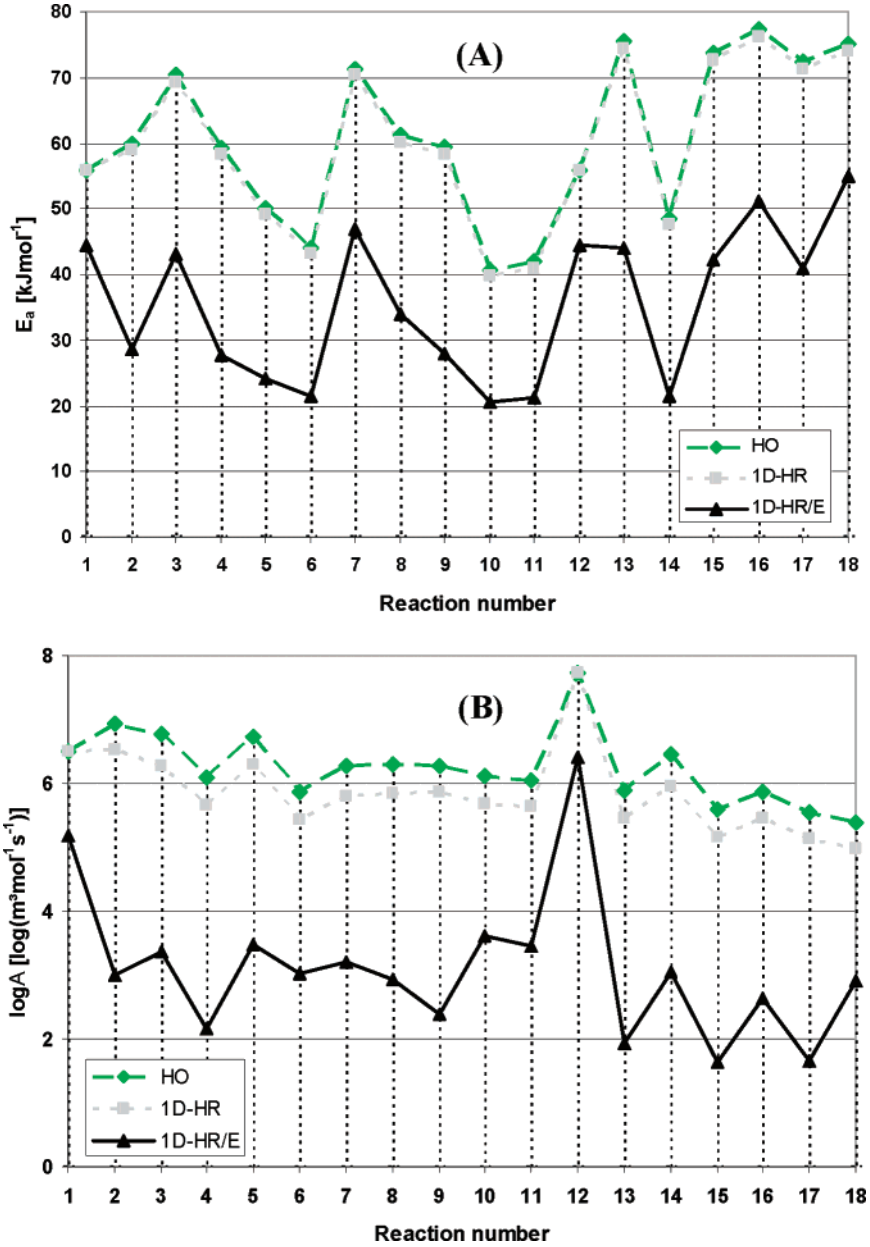

Figure 6. CBS-QB3 calculated activation energies (A) and pre-exponential factors (B) within the HO, 1D-HR, and 1D-HR/E approach at 298 K for the reactions in Table 3.

and s_o can be calculated from the classical potential energies at the reactants, saddle point, and products and from the imaginary frequency according the following five equations:

$$\alpha = -\frac{\mu 2\pi c \mathrm{Im}(\nu^{\ddagger})}{2V^{\ddagger}(V^{\ddagger} - a)} \tag{27}$$

$$a = V(s{=}+\infty) - V(s{=}-\infty) \tag{28}$$

$$b = (2V^{\ddagger} - a) + 2\sqrt{V^{\ddagger}(V^{\ddagger} - a)} \tag{29}$$

$$c = \epsilon^{\mathrm{ZPE}}(-\infty) \tag{30}$$

$$s_0 = -\frac{1}{\alpha}\ln\left(\frac{a+b}{b-a}\right) \tag{31}$$

In eq 30 $\epsilon^{\mathrm{ZPE}}(s)$ is the zero point energy as function of the reaction coordinate s. Hence c equals the zero point energy of the reactants.

List of Symbols and Acronyms

A = pre-exponential factor, $m^3\ mol^{-1}\ s^{-1}$
c = speed of light, 3.00×10^{-8} m s^{-1}
E = energy, J
E_a = activation energy, J mol^{-1}
F = second derivative matrix (Hessian)
h = Planck's constant, 6.62×10^{-34} J s
k = rate coefficient, $m^3\ mol^{-1}\ s^{-1}$
k_B = Boltzmann constant, 1.38×10^{-23} J K^{-1}
$\underline{L}$ = eigenvector matrix
$\vec{L}$ = eigenvector
n_e = number of single events
m = mass, kg
M = mass matrix, kg
P = transmission probability

q = molar partition function
R = universal gas constant, 8.314510 J mol^{-1} K^{-1}
N_A = Avogadro's constant, 6.02 × 10^{23} mol^{-1}
s = reaction coordinate, m
t = distance between the tunneling path and MEP, m
T = temperature, K
V = potential energy, J

Greek Symbols
$\kappa(s)$ = curvature, m^{-1}
$\kappa(T)$ = transmission coefficient as function of the temperature
λ = eigenvalue
Λ = eigenvalue matrix
υ = frequency, cm^{-1}
ρ = relative deviation k_{max}/k_{min} between experimental and ab initio calculated rate coefficients
θ = exponential damping of wave through energy barrier
ω = angular frequency, s^{-1}

Subscripts
calc = calculated
eff = effective reduced
exp = experimental
min = minimum
opt = optical
reac = reaction
red = reduced
max = maximum
∞ = high-pressure limit
‡ = corresponding to the transition state excluding the motion along the reaction coordinate

Superscripts
CTST = conventional transition state theory
SCTST = semiclassical transition state theory
‡ = corresponding to the transition state

Acronyms
CD-SCS = centrifugal dominant small curvature semiclassical
CTST = conventional transition state theory
FR = free rotor
1D-HR = 1D hindered internal rotor
1D-HR/E = 1D hindered internal rotor treatment with Eckart tunneling correction
1D-HR/S&T = 1D hindered internal rotor treatment with Skodje and Truhlar tunneling correction
1D-HR/W = 1D hindered internal rotor treatment with Wigner tunneling correction
HO = harmonic oscillator
IRC = intrinsic reaction coordinate
MEP = minimum energy path
SCT = small curvature tunneling
S&T = Skodje and Truhlar
TS = transition state
VTST = variational transition state theory
ZCT = zero curvature tunneling
ZPVE = zero point vibrational energy

Supporting Information Available: Tables of frequencies and rotational hindrance, activation energies, pre-exponential factors, and geometries. This material is available free of charge via the Internet at http://pubs.acs.org.

References and Notes

(1) Truhlar, D. G.; Garrett, B. C.; Klippenstein, S. J. *J. Phys. Chem.* **1996**, *100*, 12771.
(2) Truhlar, D. G.; Garrett, B. C. *Annu. Rev. Phys. Chem.* **1984**, *35*, 159.
(3) Pu, J. Z.; Truhlar, D. G. *J. Chem. Phys.* **2002**, *117*, 10675.
(4) Espinosa-Garcia, J. *J. Chem. Phys.* **2002**, *116*, 10664.
(5) Mebel, A. M.; Morokuma, K.; Lin, M. C. *J. Chem. Phys.* **1995**, *103*, 3440.
(6) Zhang, X.; Ding, Y. H.; Li, Z. S.; Huang, X. R.; Sun, C. C. *J. Phys. Chem. A* **2000**, *104*, 8375.
(7) Temelso, B.; Sherrill, C. D.; Merkle, R. C.; Freitas, R. A. *J. Phys. Chem. A* **2006**, *110*, 11160.
(8) Mebel, A. M.; Lin, M. C.; Yu, T.; Morokuma, K. *J. Phys. Chem. A* **1997**, *101*, 3189.
(9) Hemelsoet, K.; Moran, D.; Van Speybroeck, V.; Waroquier, M.; Radom, L. *J. Phys. Chem. A* **2006**, *110*, 8942.
(10) Hemelsoet, K.; Van Speybroeck, V.; Moran, D.; Marin, G. B.; Radom, L.; Waroquier, M. *J. Phys. Chem. A* **2006**, *110*, 13624.
(11) Truong, T. N.; Truhlar, D. G. *J. Chem. Phys.* **1990**, *93*, 1761.
(12) Sumathi, R.; Carstensen, H. H.; Green, W. H. *J. Phys. Chem. A* **2001**, *105*, 6910.
(13) Sumathi, R.; Carstensen, H. H.; Green, W. H. *J. Phys. Chem. A* **2001**, *105*, 8969.
(14) Coote, M. L. *J. Phys. Chem. A* **2004**, *108*, 3865.
(15) Saeys, M.; Reyniers, M. F.; Van Speybroeck, V.; Waroquier, M.; Marin, G. B. *ChemPhysChem* **2006**, *7*, 188.
(16) Donahue, N. M.; Clarke, J. S.; Anderson, J. G. *J. Phys. Chem. A* **1998**, *102*, 3923.
(17) Zavitsas, A. A.; Melikian, A. A. *J. Am. Chem. Soc.* **1975**, *97*, 2757.
(18) Zavitsas, A. A. *J. Chem. Soc., Perkin Trans. 2* **1996**, 391.
(19) Zavitsas, A. A. *J. Am. Chem. Soc.* **1998**, *120*, 6578.
(20) Blowers, P.; Masel, R. *AIChE J.* **2000**, *46*, 2041.
(21) Ma, X. L.; Schobert, H. H. *Ind. Eng. Chem. Res.* **2003**, *42*, 1151.
(22) Su, P. F.; Song, L. C.; Wu, W.; Hiberty, P. C.; Shaik, S. *J. Am. Chem. Soc.* **2004**, *126*, 13539.
(23) Hund, F. *Z. Phys.* **1927**, *43*, 805.
(24) Montgomery, J. A.; Frisch, M. J.; Ochterski, J. W.; Petersson, G. A. *J. Chem. Phys.* **1999**, *110*, 2822.
(25) Baboul, A. G.; Curtiss, L. A.; Redfern, P. C.; Raghavachari, K. *J. Chem. Phys.* **1999**, *110*, 7650.
(26) Adamo, C.; Barone, V. *J. Chem. Phys.* **1998**, *108*, 664.
(27) Boese, A. D.; Martin, J. M. L. *J. Chem. Phys.* **2004**, *121*, 3405.
(28) Chemical Kinetics Database, Standard Reference Database 17, Version 7.0 (Web Version), Release 1.3. http://kinetics.nist.gov/ 2005.
(29) Martin, J. M. L.; de Oliveira, G. *J. Chem. Phys.* **1999**, *111*, 1843.
(30) Parthiban, S.; Martin, J. M. L. *J. Chem. Phys.* **2001**, *114*, 6014.
(31) *Gaussian 03*, revision B.03; Gaussian, Inc.: Wallingford, CT, 2004.
(32) *MOLPRO*, version 2006.1, a package of ab initio programs, see http://www.molpro.net/, 2006.
(33) Saeys, M.; Reyniers, M. F.; Marin, G. B.; Van Speybroeck, V.; Waroquier, M. *J. Phys. Chem. A* **2003**, *107*, 9147.
(34) Petersson, G. A.; Allaham, M. A. *J. Chem. Phys.* **1991**, *94*, 6081.
(35) Curtiss, L. A.; Raghavachari, K.; Redfern, P. C.; Rassolov, V.; Pople, J. A. *J. Chem. Phys.* **1998**, *109*, 7764.
(36) Izgorodina, E. I.; Coote, M. L. *J. Phys. Chem. A* **2006**, *110*, 2486.
(37) Sabbe, M. K.; Vandeputte, A. G.; Reyniers, M. F.; Van Speybroeck, V.; Waroquier, M.; Marin, G. B. *J. Phys. Chem. A* **2007**, *111*, 8416.
(38) Izgorodina, E. I.; Coote, M. L.; Radom, L. *J. Phys. Chem. A* **2005**, *109*, 7558.
(39) de Oliveira, G.; Martin, J. M. L.; De Proft, F.; Geerlings, P. *Phys. Rev. A* **1999**, *60*, 1034.
(40) Berces, T. IUPAC Critical evaluation of thermochemical properties of selected radicals. Part 1. https://cmcs.ca.sandia.gov/cmcs/portal/, 2003.
(41) Andersson, M. P.; Uvdal, P. *J. Phys. Chem. A* **2005**, *109*, 2937.
(42) Van Speybroeck, V.; Van Neck, D.; Waroquier, M.; Wauters, S.; Saeys, M.; Marin, G. B. *J. Phys. Chem. A* **2000**, *104*, 10939.
(43) Van Speybroeck, V.; Vansteenkiste, P.; Van Neck, D.; Waroquier, M. *Chem. Phys. Lett.* **2005**, *402*, 479.
(44) Vansteenkiste, P.; Van Neck, D.; Van Speybroeck, V.; Waroquier, M. *J. Chem. Phys.* **2006**, *124*, Art. No. 044314.
(45) Vansteenkiste, P.; Van Neck, D.; Van Speybroeck, V.; Waroquier, M. *J. Chem. Phys.* **2006**, *125*, Art. No. 049902.
(46) East, A. L. L.; Radom, L. *J. Chem. Phys.* **1997**, *106*, 6655.
(47) Heuts, J. P. A.; Gilbert, R. G.; Radom, L. *Macromolecules* **1995**, *28*, 8771.
(48) Wigner, E. *J. Chem. Phys.* **1937**, *5*, 720.
(49) Skodje, R. T.; Truhlar, D. G.; Garrett, B. C. *J. Phys. Chem.* **1981**, *85*, 3019.
(50) Eckart, C. *Phys. Rev.* **1930**, *35*, 1303.
(51) Schwartz, M.; Marshall, P.; Berry, R. J.; Ehlers, C. J.; Petersson, G. A. *J. Phys. Chem. A* **1998**, *102*, 10074.
(52) Gonzalez, C. A.; Allison, T. C.; Louis, F. *J. Phys. Chem. A* **2001**, *105*, 11034.
(53) Truong, T. N. *J. Chem. Phys.* **1995**, *102*, 5335.

(54) Truhlar, D. G.; Isaacson, A. D.; Skodje, R. T.; Garrett, B. C. *J. Phys. Chem.* **1982**, *86*, 2252.
(55) Van Speybroeck, V.; Marin, G. B.; Waroquier, M. *ChemPhysChem* **2006**, *7*, 2205.
(56) Kungwan, N.; Truong, T. N. *J. Phys. Chem. A* **2005**, *109*, 7742.
(57) Coote, M. L.; Collins, M. A.; Radom, L. *Mol. Phys.* **2003**, *101*, 1329.
(58) NIST Chemistry webbook, Standard Reference Database 69, June 2005 Release. http://webbook.nist.gov/, 2005.
(59) Luo, Y. R. *Handbook of bond dissociation energies in organic compounds*; CRC Press: Boca Raton, FL, 2003.
(60) O'Neal, H. E.; Benson, S. W. Thermochemistry of free radicals. In *Free radicals*; Kochi, J. K., Ed.; Wiley: New York, 1973; pp 275−359.
(61) Benson, S. W.; Cruickshank, F. R.; Golden, D. M.; Haugen, G. R.; O'Neal, H. E.; Rodgers, A. S.; Shaw, R.; Walsh, R. *Chem. Rev.* **1969**, *69*, 279.